CALPHAD: Computer Coupling of Phase Diagrams and Thermochemistry 35 (2011) 601–619

Contents lists available at SciVerse ScienceDirect

CALPHAD: Computer Coupling of Phase Diagrams and Thermochemistry

journal homepage: www.elsevier.com/locate/calphad

Equilibrium between MB_2 (M = Ti, Zr, Hf) UHTC and Ni: A thermodynamic database for the B–Hf–Ni–Ti–Zr system

G. Cacciamani [a,*], P. Riani [a], F. Valenza [b]

[a] Dipartimento di Chimica e Chimica Industriale, Università di Genova, Genova, Italy

[b] Istituto per l'Energetica e le Interfasi-IENI CNR, Genova, Italy

ARTICLE INFO

Article history:
Received 3 August 2011
Received in revised form
3 October 2011
Accepted 3 October 2011
Available online 31 October 2011

Keywords:
Ultra High Temperature Ceramics
Thermodynamic database
CALPHAD
Metal–diboride joining

ABSTRACT

MB_2 (M = Ti, Zr, Hf) Ultra High Temperature Ceramics (UHTCs) are characterised by melting temperatures in excess of 3000 °C and have structural, physical, transport, and thermodynamic properties suitable for use as thermal barriers in extreme environments. It is then necessary to investigate interactions of the diborides with the materials they are supposed to protect. To this end it has been developed a CALPHAD thermodynamic database for the calculation of phase equilibria and thermodynamic properties in the quinary system B–Ni–Ti–Zr–Hf. The database contains thermodynamic parameters for all the phases included in the 10 binary and 10 ternary sub-systems of B–Ni–Ti–Zr–Hf. A few binary systems (B–Hf, B–Ti, B–Zr, Hf–Ni, Ni–Zr) have been slightly modified with respect to the previous assessments and several ternary systems (B–Hf–Ni, B–Ni–Ti, B–Ni–Zr, B–Hf–Zr, B–Ti–Zr, Hf–Ni–Ti, Hf–Ni–Zr, Hf–Ti–Zr, Ni–Ti–Zr) have been completely assessed or re-assessed in this work with particular attention to the self-consistency of the models adopted.

1. Introduction

Ultra High Temperature Ceramics (UHTCs) include materials characterised by melting temperatures often in excess of 3000 °C such as borides, carbides and nitrides of the Group 4 as well as Group 5 transition metals. Among them Ti, Zr and Hf diborides have structural, physical, transport, and thermodynamic properties which make them promising materials for use in extreme environments. In particular, the unique combination of high melting temperature, thermal conductivity, resistance to erosion, corrosion and thermal shock, makes them suitable for use in high performance applications, where high temperatures, high thermal fluxes and severe surface stresses are involved [1,2]. They can be employed, in particular, as thermal protection systems in hypersonic flight, atmospheric re-entry vehicles, and rocket propulsion [3,4], as well as in nuclear plants [5,6], refractory linings [7], electrodes [8,9], microelectronics [10], and cutting tools [11]. In view of these potential applications it is then necessary to investigate, in addition to the individual properties of these materials, their interactions with materials they are supposed to protect: metals and alloys in particular. Wettability and interfacial tension of Group 4 diborides in contact with metals as well as joining properties have been especially investigated at the IENI CNR [12–16] in two main temperature ranges, i.e. at around 1100 and 1500 °C. Results obtained from phase analysis and contact angle measurements by sessile-drop technique may be better understood if the relevant phase diagrams are known. However, most of the phase diagrams relevant to the interactions between Group 4 diborides and transition metals, e.g. nickel, are poorly known or not known at all.

Then, as a contribution to the investigation of the interaction between Group 4 diborides and nickel, a CALPHAD thermodynamic database has been developed for the calculation of phase equilibria and thermodynamic properties in the quinary system B–Ni–Ti–Zr–Hf. Though only systems containing B, Ni and one among Ti, Zr and Hf are relevant to the investigation of Ni–diboride interactions, the database contains thermodynamic parameters for all the phases included in the 10 binary and 10 ternary sub-systems of B–Ni–Ti–Zr–Hf. Particular attention has been devoted to the determination of the most appropriate thermodynamic model for the different solid phases, especially those which are stable in more systems and are characterised by more or less extended solubility ranges. When available and consistent with the present modelling, parameters already evaluated and reported in the literature have been adopted. However, for several systems, literature data were missing or inconsistent with the present modelling and more or less complete re-assessments have been performed in this work,

* Correspondence to: Dipartimento di Chimica e Chimica Industriale, Università di Genova, via Dodecaneso, 31, I-16146 Genova, Italy. Tel.: +39 010 353 6130.
E-mail address: cacciamani@chimica.unige.it (G. Cacciamani).

0364-5916/$ – see front matter © 2011 Elsevier Ltd. All rights reserved.
doi:10.1016/j.calphad.2011.10.003

with particular attention to the seven binary and three ternary subsystems containing only one among Hf, Ti and Zr.

2. Thermodynamic models

Many phases are included in the database. Their Gibbs energy is given by the sum of several contributions:

$$G^{\varphi} = {}^{ref}G^{\varphi} + {}^{id}G^{\varphi} + {}^{ex}G^{\varphi} + {}^{mag}G^{\varphi} \quad (1)$$

where ${}^{ref}G^{\varphi}$ is the reference Gibbs energy, ${}^{id}G^{\varphi}$ and ${}^{ex}G^{\varphi}$ are the ideal and excess mixing contributions, respectively, and ${}^{mag}G^{\varphi}$ is the magnetic contribution, which is only relevant when magnetic ordering occurs. Each term in the summation may assume different expressions, depending on the nature of the phase.

The different phases included in the database can be grouped according to the interaction and mixing mechanism between the component elements. Phases belonging to the same group are modelled in a similar way within the compound energy formalism (CEF).

The different groups and the corresponding thermodynamic models are briefly introduced in the following sections.

2.1. Elements

For each metallic element in the solid state, the Gibbs energy is defined, as a function of temperature, not only for the stable phases (fcc Ni, hcp and bcc Hf, Ti and Zr) but for any of the fundamental structures: fcc (cF4, Cu), bcc (cI2, W), hcp (cP2, Mg). For solid boron only the beta phase (rP105, beta-B) is considered and evaluated in this work.

The temperature dependence of the Gibbs energy of a pure component in the phase φ is generally expressed by

$$G^{\varphi}(T) = A^{\varphi} + B^{\varphi}T + C^{\varphi}T\ln T + D^{\varphi}T^2 + \cdots \quad (2)$$

where $A, B, C, D, \ldots$ are empirical parameters evaluated on the basis of the experimental information. They can be retrieved from the PURE4 database by SGTE [17]. Several temperature ranges with different sets of parameters can actually be needed to accurately describe $G^{\varphi}(T)$ in a wide temperature range.

For magnetic elements (such as Ni in the present database) Eq. (2) refers to the paramagnetic state and the ${}^{mag}G^{\varphi}$ term is added to account for magnetic ordering. It is expressed, for the pure components, according to the model introduced by Inden [18,19] and subsequently adapted by Hillert and Jarl [20]:

$${}^{mag}G^{\varphi} = RT \cdot f(\tau) \cdot \ln(\beta(x) + 1)$$

where β is the average magnetic moment per mole of atoms in Bohr magnetons, τ is the ratio T/T_C (T_C = critical temperature for magnetic ordering), and $f(\tau)$ is a polynomial expression obtained by expanding Inden's description of the magnetic heat capacity into a power series of τ. Magnetic parameters for pure elements are available in the PURE4 database by SGTE [17].

2.2. Liquid

The liquid phase is modelled as a random, disordered solution of the component elements. No experimental evidence of ionic species in the liquid is reported for the systems considered in this work. Then, it has been assumed that the constituents of the liquid phase are the neutral atomic species of the component elements. Then the liquid model is

LIQUID: (B, Hf, Ni, Ti, Zr)

where brackets represent the single thermodynamic sublattice where all components mix together. For the liquid phase only first three addenda of Eq. (1) are effective. They can be written as

$$\begin{aligned} {}^{ref}G^{\varphi} &= \sum_i x_i G_i^{\varphi}(T) \\ {}^{id}G^{\varphi} &= RT\sum_i x_i \ln x_i \\ {}^{ex}G^{\varphi} &= {}^{ex2}G^{\varphi} + {}^{ex3}G^{\varphi} + \cdots \end{aligned} \quad (3)$$

where x_i is the mole fraction of component i, $G_i^{\varphi}(T)$ is the Gibbs energy of the pure component i in the φ phase, ${}^{ex2}G^{\varphi}$ and ${}^{ex3}G^{\varphi}$ are the binary and ternary interaction terms, respectively, contributing to the excess Gibbs energy. They are expressed as

$${}^{ex2}G^{\varphi} = \sum_{i=1}^{n-1}\sum_{j=i+1}^{n} x_i x_j \sum_{\nu} {}^{\nu}L_{i,j}^{\varphi}(T)\left(x_i - x_j\right)^{\nu} \quad (4)$$

and

$$\begin{aligned} {}^{ex3}G^{\varphi} = &\sum_{i=1}^{n-2}\sum_{j=i+1}^{n-1}\sum_{k=j+1}^{n} x_i x_j x_k \\ &\times \left(u_i L_i^{\varphi}(T) + u_j L_j^{\varphi}(T) + u_k L_k^{\varphi}(T)\right) \end{aligned} \quad (5)$$

respectively, with

$$\begin{aligned} u_i &= x_i + \frac{1 - x_i - x_j - x_k}{3}, \\ u_j &= x_j + \frac{1 - x_i - x_j - x_k}{3}, \\ u_k &= x_k + \frac{1 - x_i - x_j - x_k}{3}. \end{aligned} \quad (6)$$

$L^{\varphi}(T)$ in Eqs. (4) and (5) are empirical parameters whose temperature dependence is similar to that of $G^{\varphi}(T)$ given in Eq. (2).

2.3. Disordered solid solutions (with interstitials)

When a second component is added to a metallic element, unary phases such as hcp, bcc, and fcc tend to form more or less extended disordered substitutional solid solutions. In this case temperature and composition dependence of the Gibbs free energy are those expressed in Eqs. (1)–(6).

However, when small atoms such as B are added to large early transition metals such as Ti, Zr and Hf, due to the atomic dimension mismatch, an interstitial solid solution is preferred. To be able to treat such a case, hcp, bcc and fcc phases have been described by a two-sublattice model, the first sublattice being occupied by the metallic elements and the second, usually empty, may be occupied by interstitial elements (see phases 1 to 3 in the Appendix A). The expression of the Gibbs free energy of a multi-sublattice phase is introduced later, in Section 2.5.

For a binary phase with magnetic ordering the composition dependence of ${}^{mag}G^{\varphi}$ results from the composition dependence of T_C and β, which are expressed by a Redlich–Kister series expansion:

$$\begin{aligned} T_C^{\varphi}(x) &= x_A T_C^{\varphi}(A) + x_B T_C^{\varphi}(B) + x_A x_B \sum_{\nu=0}^{n} {}^{\nu}T_C^{\varphi}\,(x_A - x_B)^{\nu} \\ \beta_C^{\varphi}(x) &= x_A \beta_C^{\varphi}(A) + x_B \beta_C^{\varphi}(B) + x_A x_B \sum_{\nu=0}^{n} {}^{\nu}\beta_C^{\varphi}\,(x_A - x_B)^{\nu} \end{aligned}$$

where ${}^{\nu}T_C^{\varphi}$ and ${}^{\nu}\beta_C^{\varphi}$ are expansion parameters to be evaluated on the basis of the experimental information available. The ${}^{mag}G^{\varphi}$ term is present only in the fcc, bcc and hcp solid solutions (phases 1 to 3 in the Appendix A) when including Ni.

2.4. Compounds

In this work the term *compound* refers to phases which do not show any solubility. This means that they are e.g. point compounds in an isobaric and isothermal binary phase diagram.

As for the modelling, a compound is represented by an n-sublattice model (where n is the number of component elements) with each sublattice occupied by only one of the component elements.

In the database several phases (see phases 5–13 in the Appendix A) are modelled as binary compounds which do not dissolve any other element.

In this case Eqs. (3) become

$$^{ref}G^{\varphi} = \sum_i x_i G_i^{SER}(T) + {}^{form}G^{\varphi}(T)$$
$$^{id}G^{\varphi} = 0$$
$$^{ex}G^{\varphi} = 0$$

where $G_i^{SER}(T)$ is the Gibbs energy of the pure component i in its standard element reference (SER) state and $^{form}G^{\varphi}(T)$ is the Gibbs energy of formation of the compound expressed, as a function of temperature, according to Eq. (2).

2.5. Ordered solid solutions

Ordered solid solutions are binary or higher order intermediate phases showing more or less extended solution ranges. Similarly to compounds each component element occupies a preferential site, but mixing of different elements in the same site is allowed, as well as appearance of vacancies. Contrary to the disordered solutions (such as those based on the pure components) ordered solutions must be modelled by two or more sublattices, one or more of which are occupied by two or more different components. Two typical situations may be distinguished:

(1) Each sublattice may be occupied by more elements, but each component element can occupy only one sublattice. With such a restriction on the substitution mechanism only line ternary, surface quaternary, etc. solutions may be formed. In general, for n component phases described in this way, solubility ranges can be $(n-1)$ dimensional or lower (see phases 14–20 in the Appendix A).
(2) Each component element can occupy two or more (possibly all) sublattices (see phases 21–30 in the Appendix A). A typical example may be an ordered binary solution represented by a two-sublattice model where each sublattice is mainly occupied by one of the component elements but reciprocal substitution between the elements is allowed. Then both elements can occupy both sublattices. When a new component is added, it will preferentially occupy one of the sublattices, but it will also be allowed to occupy the other one.

In some cases vacancies, in addition to reciprocal substitution between components, contribute to the non-stoichiometry of a phase. Notice that they appear as sublattice constituents as well as atomic species do (see phases 1–3, 21, 24–26 in the Appendix A).

Whenever more components are allowed to mix in two or more sublattices the Gibbs energy is expressed as a function of the site fractions $y_i^{(s)}$, the mole fractions of each component i in the sublattice s. Site fractions obey the conditions

$$\sum_i y_i^{(s)} = 1$$
$$\frac{\sum_s n^{(s)} y_i^{(s)}}{\sum_s n^{(s)}(1 - y_{VA})} = x_i$$

where $n^{(s)}$ are the stoichiometric coefficients relating the sublattices. Eqs. (3) become

$$\begin{aligned}
^{ref}G^{\varphi} &= \sum_i \sum_j \cdots \sum_k y_i^{(1)} y_j^{(2)} \cdots y_k^{(s)} G^{\varphi}_{i:j:\cdots:k} \\
^{id}G^{\varphi} &= \frac{1}{\sum_s n^{(s)}} RT \sum_s \sum_i n^{(s)} y_i^{(s)} \ln y_i^{(s)} \\
^{ex}G^{\varphi} &= {}^{ex2}G^{\varphi} + {}^{ex3}G^{\varphi} + \cdots \\
&= \sum_s \sum_i \sum_j y_i^{(s)} y_j^{(s)} \sum_{r \neq s} \sum_k y_k^{(s)} L^{\varphi}_{i:j:\cdots:k}(T) \\
&\quad + \cdots + {}^{ex3}G^{\varphi} + \cdots
\end{aligned} \tag{7}$$

where $G^{\varphi}_{i:j:\cdots:k}$ in $^{ref}G^{\varphi}$ are the Gibbs energies of all the so-called "end members", the stoichiometric compounds (either stable, metastable or unstable) formed when only one constituent is present in each sublattice. $L^{\varphi}_{i:j:\cdots:k}(T)$ in $^{ex2}G^{\varphi}$ are interaction parameters corresponding to the mixing of components i and j on the sublattice s while the other sublattices are singly occupied. More terms can be added to $^{ex2}G^{\varphi}$, corresponding to simultaneous mixing on two sublattices while the remaining sublattices are singly occupied. $^{ex3}G^{\varphi}$ accounts for the possible interactions of three elements in a given sublattice and it was never needed in the present database.

A special case occurs when an ordered solid solution is structurally related to a disordered phase. This is the case of, say, CsCl and W type (bcc) phases. Such phases are described by a single multi-sublattice model where all involved atoms can occupy all the sublattices. The occupation of the different sublattices, which determines the ordered or disordered state of the phase, results from the equilibrium calculations. In the present database two phases have been described in this way: metastable $TiNi_3$ with the $AuCu_3$ type structure, related to disordered fcc, and TiNi with the CsCl structure, related to bcc (see phases 29 and 30 in the Appendix A).

In this case the Gibbs energy of the related phases is given by a single expression

$$G^{\varphi} = {}^{dis}G^{\varphi}(x_i) + \Delta^{ord}G^{\varphi}(y_i^{(s)})$$

where $^{dis}G^{\varphi}(x_i)$ is the Gibbs energy of the disordered state, given by Eqs. (3)–(6), while the ordering contribution to the Gibbs energy

$$\Delta^{ord}G^{\varphi}(y_i^{(s)}) = G^{\varphi}(y_i^{(s)}) - G^{\varphi}(y_i^{(s)} = x_i)$$

is given by the difference between two contributions expressed according to Eqs. (7), first calculated using the actual site occupations and then replacing the actual site fractions by the global phase compositions, which corresponds to a disordered state.

3. Results and discussion

In order to built a self-consistent B–Hf–Ni–Ti–Zr thermodynamic database, as a first step, all the relevant solid phases have been considered and, for each one, the most appropriate model has been selected. They have been introduced in the previous section and listed in the Appendix A.

As a second step all thermodynamic assessments available in the literature have been considered and tested: first of all for consistency with the phase models adopted, then for mutual compatibility and predictive ability. In a number of systems where different phase models had been used in the literature, re-modelling was carried out by simple conversion of the parameters or, when necessary, by partial reassessment. Then, when more assessments were available for the same system, the most appropriate was selected by considering its compatibility with the assessments already selected and its ability to give better extrapolations to higher order systems when added to the database.

Table 1
Selected invariant B–Hf equilibria calculated in this work.

Reaction	Type	1st phase x (Hf)	2nd phase x (Hf)	3rd phase x (Hf)	Temp. (°C)
$L \rightleftarrows HfB_2$	Congruent	0.333	0.333	–	3378
$L + HfB_2 \rightleftarrows HfB$	Peritectic	0.781	0.333	0.500	2104
$L \rightleftarrows HfB_2 + B$	Eutectic	0.010	0.323	0.0	2065
$L \rightleftarrows HfB + bcc\text{-}Hf$	Eutectic	0.850	0.500	0.990	1881
$HfB + bcc\text{-}Hf \rightleftarrows hcp\text{-}Hf$	Peritectoid	0.500	0.993	0.985	1790

For a number of systems no satisfactory assessment or no assessment at all was found in the literature and a complete assessment (or re-assessment) was carried out in this work.

All the interaction parameters included in the B–Hf–Ni–Ti–Zr database are summarised in the Appendix B. In the following sections all binary and ternary systems included in the database are briefly presented and discussed.

3.1. B–Hf

The B–Hf phase diagram has been experimentally investigated by Rudy et al. [21] and Portnoi et al. [22] and critically assessed by Okamoto [23].

Main features of the phase diagram are: the very high melting point of HfB_2 (3380 °C) and the peritectic formation of HfB (which was considered not a stable phase by Portnoi et al. [22]). B–Hf binary phases are listed here below:

Formula	*Pearson symbol, prototype, structurbericht*	*Phase model (see* the Appendix A and Section 2)
HfB_2	hP3, AlB_2, C32	ALB2_TY
HfB	oP8, FeB, B27	FEB_TY

Several authors experimentally investigated thermodynamics of the B–Hf compounds: enthalpy, entropy and heat capacity data from the literature have been summarised and discussed by Bittermann and Rogl [24]. A cursory CALPHAD assessment of the system was first published by Rogl and Potter [25] and subsequently improved by Bittermann and Rogl [24]. Both Refs. [25,24] preferred phase diagram data from Rudy and Windisch [21] even if DTA data of [21,22] are in good agreement. B solubility in Hf was described by Bittermann and Rogl [24] as interstitial type, based on the increase in the lattice parameters of α-Hf with respect to the pure metal. However, the solubility range of the intermediate compounds was neglected.

Parameters calculated by Bittermann and Rogl [24] are adopted in this work. In addition, the narrow solubility range of HfB_2 has been modelled by assuming that vacancies may be present in the metal sublattice. The phase diagram calculated in this work is reported in Fig. 1. Moreover, calculated temperatures and compositions of selected invariant reactions are listed in Table 1.

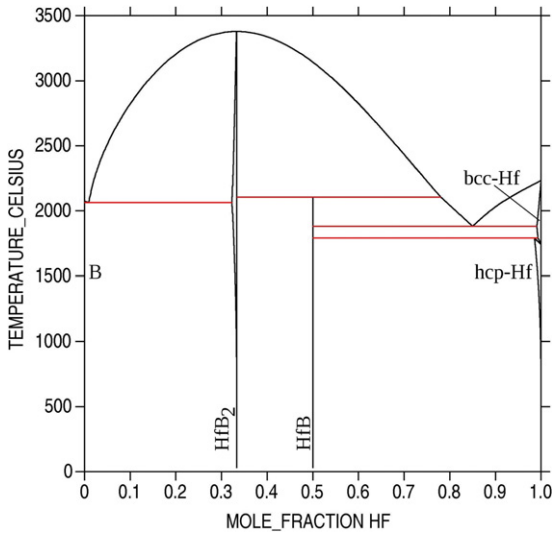

Fig. 1. The calculated B–Hf phase diagram.

3.2. B–Ni

The B–Ni phase diagram has been experimentally investigated by several authors and critically assessed by Liao and Spear [26], based on the literature until 1988. Five B–Ni intermediate compounds have been reported:

Formula	*Pearson symbol, prototype, structurbericht*	*Phase model (see* the Appendix A and Section 2)
NiB	oC8, CrB, B_f	CRB_TY
m-Ni_4B_3	mC*, -, -	M–NI4B3
o-Ni_4B_3	oP*, -, -	O–NI4B3
Ni_2B	tI12, Al_2Cu, C16	CUAL2_TY
Ni_3B	oP16, Fe_3C, $D0_{11}$	NI3B

Three of them melt congruently at temperatures well below the average melting temperature of the component elements. Two of them, o-Ni_4B_3 and m-Ni_4B_3, show off-stoichiometric compositions of 41.5 at.% and 43.5 at.% B, respectively. NiB_2 and NiB_{12} reported in the literature by some authors, have not been confirmed as stable phases by the experiments of [27].

After a first CALPHAD assessment done by Hack and Chart [28], the system was re-assessed by Teppo and Taskinen [29] and revised by Campbell and Kattner [30] who, in particular, re-modelled the B solubility in fcc-Ni from substitutional to interstitial.

More recently, a new assessment has been published by Sun et al. [27], based on first principles calculations and new experiments about the B solubility in Ni and the liquidus around the Ni_4B_3 compounds. However, the Gibbs energy expression used by Sun et al. [27] for B in the fcc structure is different from that reported in the PURE4 database and accepted in this work. For this reason the interaction parameters calculated by Campbell and Kattner [30] are here preferred, also considering that there is no significant difference between the two phase diagrams. The phase diagram calculated in this work is reported in Fig. 2 while temperatures and phase compositions for selected invariant reactions are reported in Table 2. It may be observed that, as usual for phases very close in composition, only one of the two Ni_4B_3 compounds is stable down to low temperature.

3.3. B–Ti

Experimental investigations of the B–Ti phase diagram have been critically assessed by Murray et al. [31]. Main features of the phase diagram are: the very high melting point of TiB_2 (3225 °C) and the peritectic formation of Ti_3B_4 and TiB. More recent DTA measurements performed by Witusiewicz et al. [32] substantially confirmed the phase diagram assessed by Murray et al. [31] except for the peritectic formation of Ti_3B_4 and TiB, which resulted to be about 60 °C lower than that reported by Murray et al. [31].

Table 2
Selected invariant B–Ni equilibria calculated in this work.

Reaction	Type	1st phase x (Ni)	2nd phase x (Ni)	3rd phase x (Ni)	Temp. (°C)
$L \rightleftarrows Ni_3B$	Congruent	0.750	0.750	–	1162
$L \rightleftarrows Ni_2B$	Congruent	0.667	0.667	–	1112
$L \rightleftarrows Ni_2B + Ni_3B$	Eutectic	0.680	0.667	0.750	1110
$L \rightleftarrows Ni_3B + Ni$	Eutectic	0.839	0.750	0.999	1088
$L + B \rightleftarrows NiB$	Peritectic	0.500	0.0	0.500	1033
$L \rightleftarrows m\text{–}Ni_4B_3$	Congruent	0.565	0.565	–	1025

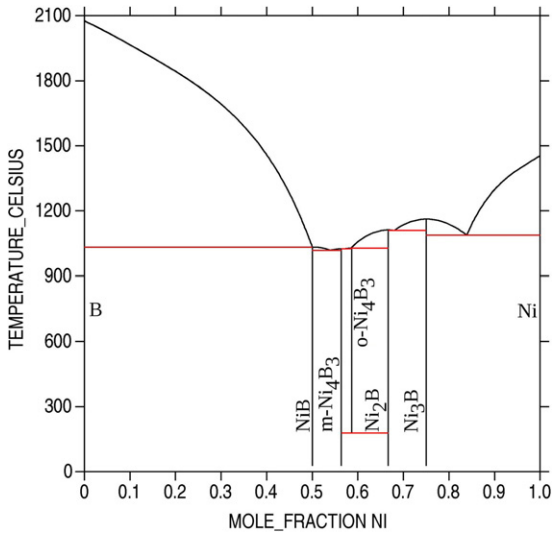

Fig. 2. The calculated B–Ni phase diagram.

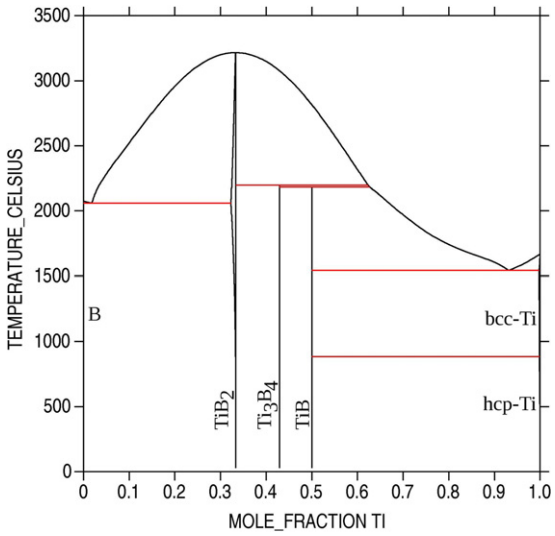

Fig. 3. The calculated B–Ti phase diagram.

Formula	*Pearson symbol, prototype, structurbericht*	*Phase model (see* the Appendix A and Section 2)
TiB_2	hP3, AlB_2, C32	ALB2_TY
Ti_3B_4	oI14, Ta_3B_4, $D7_n$	TI3B4
TiB	oP8, FeB, B27	FEB_TY

Several authors experimentally investigated thermodynamics of the B–Ti compounds: in particular enthalpy, entropy and heat capacity data were reported. These data have been summarised and discussed by Witusiewicz et al. [32]. Thermodynamics of formation of TiB_2 has been recently confirmed by EMF measurements [33].

A first CALPHAD assessment done by Baetzner [34] was improved by Bittermann and Rogl [24] by modelling the B solubility in α- and β-Ti as interstitial and adding the Ti_3B_4 phase, previously missing. Subsequently the system was reassessed by Ma et al. [35] who modelled TiB and TiB_2 as substitutional solid solutions. Finally Witusiewicz et al. [32] produced a new assessment based also on his own new experiments. Results by Bittermann and Rogl [24] are generally preferred in this work because they give better extrapolations to higher order systems when combined with the other accepted optimisations. However, by analogy with B–Hf, vacancies have been included in the metal sublattice of TiB_2 to be able to reproduce its narrow solubility range. The phase diagram calculated in this work is reported in Fig. 3 while temperatures and phase compositions for selected invariant reactions are reported in Table 3.

3.4. B–Zr

Several experimental investigations of the B–Zr phase diagram have been reported and critically assessed by Okamoto [36]. As for B–Hf and B–Ti, the phase diagram is dominated by the very high melting compound ZrB_2 (3244 °C). Two more phases, ZrB_{12} and ZrB, are only stable in limited temperature ranges. Unless the crystal structure of ZrB was experimentally determined as NaCl-type by some authors [37–39], according to the first principles total energy calculations by Tokunaga et al. [40] the FeB-type structure should be more stable.

Formula	*Pearson symbol, prototype, structurbericht*	*Phase model (see* the Appendix A and Section 2)
ZrB_{12}	cF52, UB_{12}, $D2_f$	ZRB12
ZrB_2	hP3, AlB_2, C32	ALB2_TY
ZrB	cF8, NaCl, B1 (or FeB-type?)	ZRB

As for thermodynamics, the only available data are enthalpy of formation and heat capacity of ZrB_2. After a first rough CALPHAD assessment done by Rogl and Potter [25], the system was reassessed by several authors [41,40,42]. The modelling by Tokunaga et al. [40], also supported by total energy first principles calculations, has been adopted in this work and slightly improved by modelling the narrow solubility range of ZrB_2 by assuming that vacancies may be present in the metal sublattice. As for the ZrB compound, it has been considered NaCl type, waiting for an experimental confirmation of the first principles total energy calculations by Tokunaga et al. [40]. The phase diagram calculated in this work is reported in Fig. 4 while temperatures and phase compositions for selected invariant reactions are reported in Table 4.

3.5. Hf–Ni

The critical assessment by Nash and Nash [43] was mainly based on experimental investigations by Svechnikov et al. [44] and Bsenko [45]. Afterwards Yeremenko et al. [46] reinvestigated the Hf rich part of the diagram determining, in particular, the congruent melting of the Hf_2Ni phase at 1220 °C. Okamoto [47] then redrew the phase diagram according to [46] in the 0–50 at.% Ni range and according to [43] in the Ni-rich part. Several intermediate compounds (listed here below) are present in this

Table 3
Selected invariant B–Ti equilibria calculated in this work.

Reaction	Type	1st phase x (Ti)	2nd phase x (Ti)	3rd phase x (Ti)	Temp. (°C)
$L \rightleftarrows TiB_2$	Congruent	0.333	0.333	–	3216
$L + TiB_2 \rightleftarrows Ti_3B_4$	Peritectic	0.623	0.333	0.429	2199
$L + Ti_3B_4 \rightleftarrows TiB$	Peritectic	0.627	0.429	0.500	2184
$L \rightleftarrows B + TiB_2$	Eutectic	0.018	0.0	0.333	2060
$L \rightleftarrows TiB$ + bcc-Ti	Eutectic	0.931	0.500	0.998	1541

Table 4
Selected invariant B–Zr equilibria calculated in this work.

Reaction	Type	1st phase x (Zr)	2nd phase x (Zr)	3rd phase x (Zr)	Temp. (°C)
$L \rightleftarrows ZrB_2$	Congruent	0.333	0.333	–	3243
$L + ZrB_2 \rightleftarrows ZrB_{12}$	Peritectic	0.062	0.325	0.077	2089
$L \rightleftarrows B + ZrB_{12}$	Eutectic	0.033	0.0	0.077	2026
$L \rightleftarrows ZrB_2$ + bcc-Zr	Eutectic	0.865	0.333	0.990	1690
ZrB_2 + bcc-Zr $\rightleftarrows$ ZrB	Peritectoid	0.333	0.999	0.500	1188

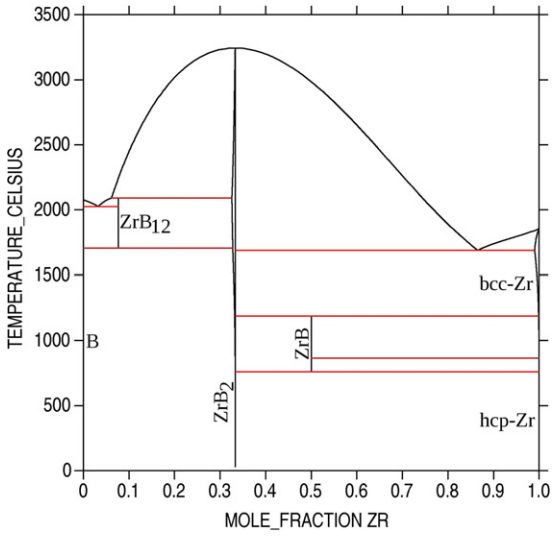

Fig. 4. The calculated B–Zr phase diagram.

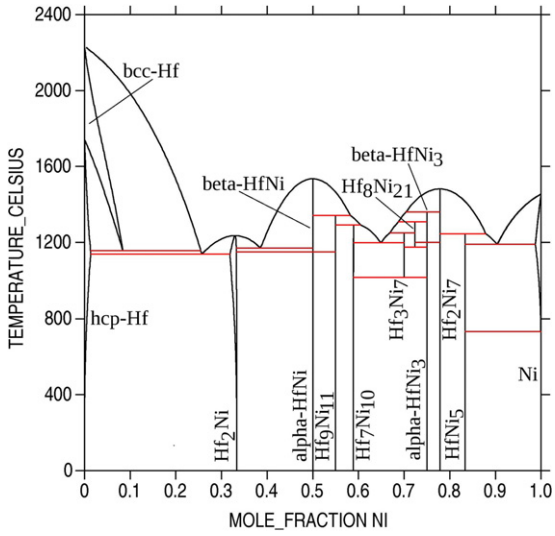

Fig. 5. The calculated Hf–Ni phase diagram.

system: a few of them are stable only in limited high temperature ranges, three of them, Hf_2Ni, β-HfNi and Hf_2Ni_7, are congruent melting. The liquidus curve runs at temperatures below the average melting temperature of the component elements.

Formula	*Pearson symbol, prototype, structurbericht*	*Phase model (see* the Appendix A and Section 2)
Hf_2Ni	tI12, Al_2Cu, C16	CUAL2_TY
β-HfNi	,,	B_HFNI
α-HfNi	oC8, CrB, B_f	CRB_TY
Hf_9Ni_{11}	tI40,,	ET9NI11
Hf_7Ni_{10}	oC68,,	ET7NI10
Hf_3Ni_7	aP20,,	HF3NI7
Hf_8Ni_{21}	aP29,,	ET8NI21
β-$HfNi_3$	hP40,,	B_HFNI3
α-$HfNi_3$	hR12, $BaPb_3$,	A_HFNI3
Hf_2Ni_7	mC36,,	ET2NI7
$HfNi_5$	cF24, $AuBe_5$, $C15_b$	AUBE5_TY

Thermodynamics of the Ni-rich liquid has been investigated by Selhaoui et al. [48] while enthalpy of formation of the solid compounds has been measured by several authors [48–50].

A first CALPHAD assessment performed by Zeng and Jin [51] was improved by Wang et al. [52]. Wang's results are here generally adopted except for selected liquid mixing parameters which have been amended in this work. The phase diagram calculated in this work is reported in Fig. 5 while temperatures and phase compositions for selected invariant reactions are reported in Table 5.

3.6. Hf–Ti

The two elements show complete solubility both in the liquid and the solid state at high temperature with both hcp(Hf, Ti) + bcc(Hf, Ti) and bcc(Hf, Ti) + liquid two-phase fields showing a minimum, as indicated by several experimental investigations summarised by Murray [53] and, more recently, by Bittermann and Rogl [24].

No thermodynamic measurements are available for this system.

A first cursory CALPHAD assessment carried out by Murray [53] was subsequently improved by Bittermann et al. [24] who assumed that a miscibility gap appears in the hcp solid solution at temperatures lower than 227 °C. Thermodynamic parameters calculated by Bittermann and Rogl [24] are adopted in this work. The phase diagram calculated in this work is reported in Fig. 6 while temperatures and phase compositions for selected invariant reactions or critical points are reported in Table 6.

3.7. Hf–Zr

According to the critical assessment by Abriata et al. [54] the two elements show complete solubility both in the liquid and solid state with narrow and monotonic two-phase fields suggesting that mixing is very close to an ideal behaviour in all phases.

Table 5
Selected invariant Hf–Ni equilibria calculated in this work.

Reaction	Type	1st phase x (Ni)	2nd phase x (Ni)	3rd phase x (Ni)	Temp. (°C)
$L \rightleftarrows \beta$-HfNi	Congruent	0.500	0.500	–	1535
$L \rightleftarrows Hf_2Ni_7$	Congruent	0.778	0.778	–	1481
$L \rightleftarrows Hf_2Ni$	Congruent	0.333	0.333	–	1235
bcc-Hf $\rightleftarrows$ hcp-Hf + L	Metatectic	0.029	0.004	0.101	1157
$L \rightleftarrows$ hcp-Hf + Hf_2Ni	Eutectic	0.257	0.013	0.333	1139
$L \rightleftarrows Hf_2Ni + \beta$-HfNi	Eutectic	0.386	0.332	0.500	1170
$L \rightleftarrows Hf_7Ni_{10} + Hf_3Ni_7$	Eutectic	0.649	0.589	0.700	1197
$L \rightleftarrows HfNi_5$ + Ni	Eutectic	0.904	0.833	0.987	1189

Table 6
Selected invariant and critical Hf–Ti equilibria calculated in this work.

Reaction	Type	1st phase x (Ti)	2nd phase x (Ti)	3rd phase x (Ti)	Temp. (°C)
$L \rightleftarrows$ bcc-(Hf, Ti)	Congruent	0.880	0.880	–	1653
bcc-(Hf, Ti) $\rightleftarrows$ hcp-(Hf, Ti)	Congruent	0.780	0.780	–	790
hcp − (Hf, Ti)	Critical pt.	0.500	–	–	227

No thermodynamic measurements are available for this system.

A CALPHAD assessment of the system was carried out by Bittermann et al. [55] who assumed an ideal mixing in the hcp solid solution and calculated interaction parameters for the bcc and liquid solutions. Their results are adopted in this work. The Hf–Zr phase diagram calculated in this work is reported in Fig. 7. No invariant equilibrium is present in this system.

3.8. Ni–Ti

Experimental investigations of the Ni–Ti phase equilibria have been critically assessed by Murray [56]. Terminal bcc solid solutions show up to 10% solubility on both Ni and Ti sides while hcp-Ti has a very low solubility for Ni. Three intermetallic compounds are formed: $TiNi_3$ and TiNi melt congruently and show appreciable solid solubility while Ti_2Ni forms peritectically. At equiatomic composition and low temperature (< 80 °C) a martensitic phase with a B19′ structure is formed giving rise to the well-known shape-memory effect of the TiNi phase.

Formula	*Pearson symbol, prototype, structurbericht*	*Phase model (see* the Appendix A and Section 2)
$TiNi_3$	hP16, $TiNi_3$, $D0_{24}$	NI3TI
$TiNi_3$	cP4, $AuCu_3$, $L1_2$ (metastable)	FCC2
TiNi	cP2, CsCl, B2	BCC2
TiNi	mP2,, B19′	Not modelled
Ti_2Ni	cF96,,	NITI2

Murray [56] assessed thermochemical data for this system, which include Gibbs energy of formation of the different solid phases and enthalpy of mixing of the liquid phase. More recently, two new investigations of the enthalpy of mixing have been performed by Lück et al. [57] and Thiedemann et al. [58].

Thermodynamic assessments for this system were performed by Bellen et al. [59], Tang et al. [60], Tokunaga et al. [61] and, finally, by De Keyzer et al. [62] who improved phase models and parameters of [59]. In particular [62] modelled the TiNi phase as a two-sublattice ordered form of the bcc solid solution and the metastable $TiNi_3$ $AuCu_3$ type as a two-sublattice ordered form of the fcc solid solution. Results by De Keyzer et al. [62] have been adopted in this work.

The Ni–Ti phase diagram calculated in this work is reported in Fig. 8 while temperatures and phase compositions for selected invariant reactions are reported in Table 7.

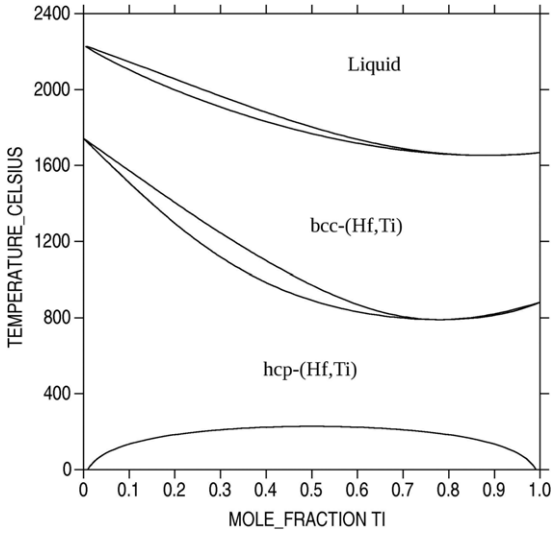

Fig. 6. The calculated Hf–Ti phase diagram.

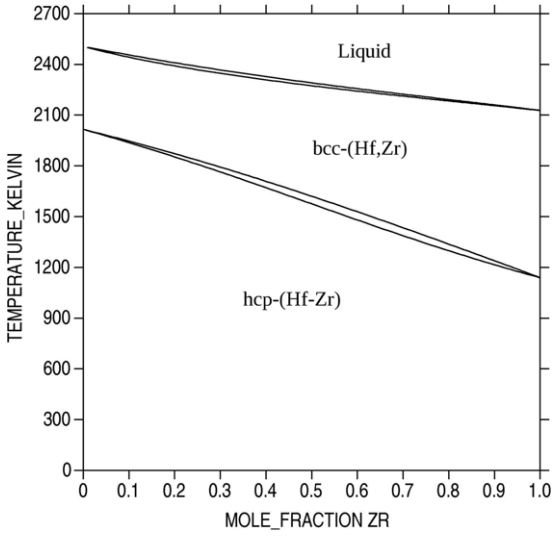

Fig. 7. The calculated Hf–Zr phase diagram.

3.9. Ni–Zr

Experimental results about the Ni–Zr phase equilibria have been critically assessed by Nash et al. [63] and selected equilibria have been recently revised by Wang et al. [64]. The system

Table 7
Selected invariant Ni–Ti equilibria calculated in this work.

Reaction	Type	1st phase *x* (Ti)	2nd phase *x* (Ti)	3rd phase *x* (Ti)	Temp. (°C)
$L \rightleftarrows TiNi_3$	Congruent	0.250	0.250	–	1384
$L \rightleftarrows TiNi$	Congruent	0.500	0.500	–	1309
$L \rightleftarrows Ni + TiNi_3$	Eutectic	0.168	0.151	0.208	1299
$L \rightleftarrows TiNi_3 + TiNi$	Eutectic	0.377	0.251	0.438	1119
$L + TiNi \rightleftarrows Ti_2Ni$	Peritectic	0.669	0.507	0.667	985
$L \rightleftarrows Ti_2Ni$ + bcc-Ti	Eutectic	0.746	0.667	0.894	942
bcc-Ti $\rightleftarrows Ti_2Ni$ + hcp-Ti	Eutectoid	0.947	0.667	0.998	767

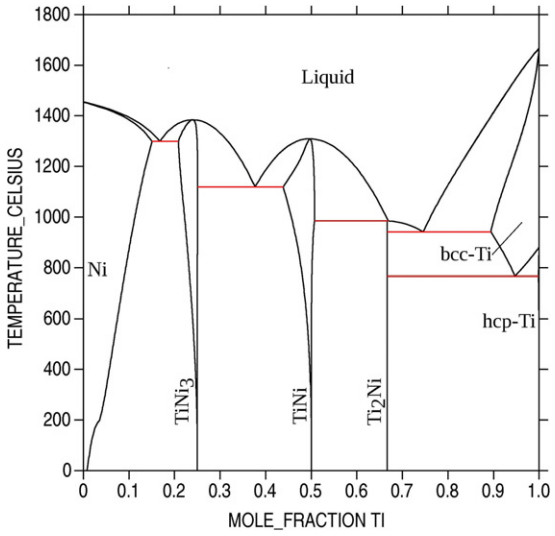

Fig. 8. The calculated Ni–Ti phase diagram.

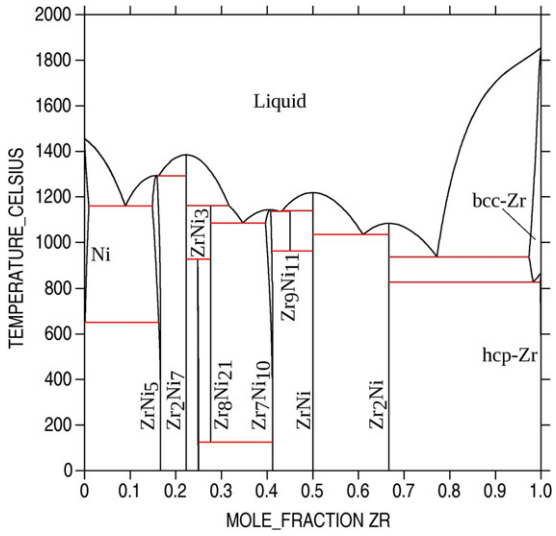

Fig. 9. The calculated Ni–Zr phase diagram.

is characterised by several intermediate compounds: three of them, Zr_2Ni_7, ZrNi and Zr_2Ni, are reported to melt congruently at temperatures below the averaged melting temperature of the component elements; two of them, Zr_7Ni_{10} and $ZrNi_5$, shows an appreciable solubility range.

Formula	*Pearson symbol, prototype, structurbericht*	*Phase model (see* the Appendix A and Section 2)
$ZrNi_5$	cF24, $AuBe_5$, $C15_b$	AUBE5_TY
Zr_2Ni_7	mC36,,	ET2NI7
$ZrNi_3$	hP8, Ni_3Sn, $D0_{19}$	NI3ZR1
Zr_8Ni_{21}	aP29,,	ET8NI21
Zr_7Ni_{10}	oC68,,	ET7NI10
Zr_9Ni_{11}	tI40,,	ET9NI11
ZrNi	oC8, CrB, B_f	CRB_TY
Zr_2Ni	tI12, Al_2Cu, C16	CUAL2_TY

Thermodynamic properties of both liquid and solid phases have been investigated by several authors: literature data are summarised and discussed by Wang et al. [64].

A CALPHAD assessment of the system was carried out by Ghosh [65] and subsequently independently improved by Tokunaga et al. [66] and Wang et al. [64]. Parameters calculated by Tokunaga et al. [66] are preferred and have been generally adopted with the exception of a few phases (e.g. Zr_7Ni_{10} and $ZrNi_3$) which have been re-modelled.

The Ni–Zr phase diagram calculated in this work is reported in Fig. 9 while temperatures and phase compositions for selected invariant reactions are reported in Table 8.

3.10. Ti–Zr

Ti and Zr show complete solubility both in the liquid and solid states. Both hcp(Hf, Ti) + bcc(Hf, Ti) and bcc(Hf, Ti) + liquid two-phase fields show a minimum at intermediate compositions. The Ti–Zr phase diagram was critically assessed by Murray [67]. No invariant three-phase equilibrium is present in the system.

Thermodynamic measurements of the enthalpy of mixing in the liquid phase have been carried out by Thiedemann et al. [68].

A CALPHAD assessment of the system has been carried out by Hari Kumar et al. [69]. According to [69] a miscibility gap appears in the hcp solid solution at low temperature: it has not been observed experimentally but it is consistent with the similar assumption adopted in the Hf–Ti assessment. More recently, the system has been re-assessed by Turchanin et al. [70] taking also into account the results by Thiedemann et al. [68]. However, parameters by Hari Kumar et al. [69] give better extrapolations when combined with the rest of the database and have been preferred.

The Ti–Zr phase diagram calculated in this work is reported in Fig. 10 while temperatures and phase compositions for selected invariant reactions or critical points are reported in Table 9.

3.11. B–Hf–Ni

The B–Hf–Ni system is only partially known: Kuzma [71] determined the 800 °C isothermal section in the whole composition range, while, in the Ni-rich corner, the same isothermal section and the liquidus monovariant lines had been previously investigated by Stadelmaier et al. [72]. Finally, a partial vertical section between pure Ni and the $Hf_2Ni_{21}B_6$ ternary compound was investigated by Lugscheider et al. [73].

No thermodynamic measurements have been done in this system.

The first CALPHAD assessment of the B–Hf–Ni system has been published very recently by Kaufman et al. [74]. Ternary equilibria computed by Kaufman et al. [74] were very helpful to understand results of wetting experiments conducted by Passerone et al. [75]. However B–Hf–Ni calculated by Kaufman

Table 8
Selected invariant Ni–Zr equilibria calculated in this work.

Reaction	Type	1st phase x (Zr)	2nd phase x (Zr)	3rd phase x (Zr)	Temp. (°C)
$L \rightleftarrows Zr_2Ni_7$	Congruent	0.222	0.222	–	1385
$L \rightleftarrows ZrNi$	Congruent	0.500	0.500	–	1219
$L \rightleftarrows Zr_2Ni$	Congruent	0.667	0.667	–	1084
$L \rightleftarrows Ni + ZrNi_5$	Eutectic	0.090	0.010	0.149	1159
$L \rightleftarrows Zr_8Ni_{21} + Zr_7Ni_{10}$	Eutectic	0.346	0.276	0.396	1086
$L \rightleftarrows ZrNi + Zr_2Ni$	Eutectic	0.610	0.500	0.667	1034
$L \rightleftarrows Zr_2Ni + bcc - Zr$	Eutectic	0.772	0.667	0.973	937

Table 9
Selected invariant and critical Ti–Zr equilibria calculated in this work.

Reaction	Type	1st phase x (Zr)	2nd phase x (Zr)	3rd phase x (Zr)	Temp. (°C)
$L \rightleftarrows$ bcc-(Ti, Zr)	Congruent	0.350	0.350	–	1553
bcc-(Ti, Zr) $\rightleftarrows$ hcp-(Ti, Zr)	Congruent	0.500	0.500	–	600
hcp-(Ti,Zr)	Critical pt.	0.500	–	–	36

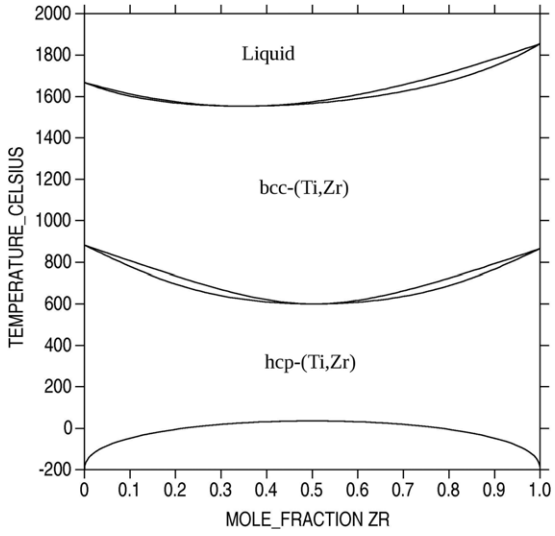

Fig. 10. The calculated Ti–Zr phase diagram.

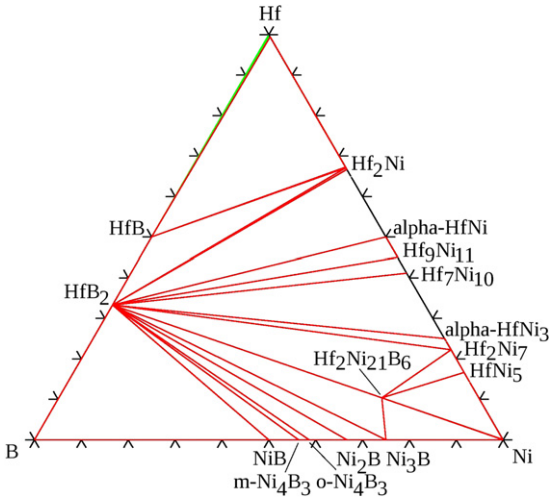

Fig. 11. The calculated B–Hf–Ni isothermal section at 800 °C.

et al. [74] was based on binary subsystems incompatible with the present database. For this reason B–Hf–Ni ternary parameters for the liquid phase and the ternary compound $Hf_2Ni_{21}B_6$ have been re-evaluated in this work. Moreover the sublattice model for the ternary phase $Hf_2Ni_{21}B_6$ has been modified in order to be more consistent with its crystal structure, reported as $Cr_{23}C_6$ type. In this structure three different sets of equivalent positions are occupied with atomic ratios 3:20:6. Then a three-sublattice model has been introduced $(Hf\%, Ni)_3\ (Hf, Ni\%)_{20}\ (B)_6$ consistently with the crystallographic sublattices. The same phase indeed, which is present in B–Ni–Ti and B–Ni–Zr, has been reported as $Ti_3Ni_{20}B_6$ in B–Ni–Ti [76]. Actually a narrow solubility range due to a reciprocal substitution between Hf and Ni has been reported in the literature, which may explain the difference between experimental (2:21:6) and crystallographic (3:20:6) stoichiometry. In the present thermodynamic modelling, however, no mixing parameters have been introduced and the $Hf_2Ni_{21}B_6$ phase has then been treated as a stoichiometric compound at the $Hf_3Ni_{20}B_6$ composition.

Results of the present assessment are summarised in Figs. 11 and 12. In Fig. 11 the 800 °C isothermal section is reported. A good agreement with experiments is observed with a few exceptions: (a) the HfB phase, missing in [71], is present in the section; (b) the Hf_3Ni_7 phase, reported by Kuzma [71], is not stable at this temperature according to the accepted Hf–Ni phase diagram; (c) the $HfB_2 + Ni_3B$ two-phase equilibrium is more stable than $Hf_2Ni_{21}B_6 + Ni_2B$ reported by both [71,72]; (d) the $Hf_2Ni_7 + Hf_2Ni_{21}B_6$ two-phase equilibrium is more stable than $Hf_2Ni_{21}B_6 + HfNi_3$, in agreement with [72] but in contradiction to [71].

The projection of the liquidus surface is reported in Fig. 12(a). Calculated liquid monovariant lines (reported in Fig. 12(b)) are in reasonable agreement with experiments by Stadelmaier and Shoemaker [72] conducted in the Ni-rich corner and including the primary solidification range of $Hf_2Ni_{21}B_6$. Characteristic features of the projection are as follows: (a) the large primary solidification area of HfB_2 and the steepness of its liquidus surface, (b) the deep valley close to the Hf–Ni binary subsystem which includes the lowest ternary eutectic of the system: Liquid $\rightleftarrows HfB_2 + \alpha$-$HfNi_3 + Hf_7Ni_{10}$ at 865 °C. All the invariant equilibria involving liquid are summarised in Table 10.

The isopleth between HfB_2 and Ni is shown in Fig. 13. The computed liquidus curve is in good agreement with experimental results by Lugscheider and Reimann [73] in the range between pure Ni and the $Hf_2Ni_{21}B_6$ ternary compound.

3.12. B–Ni–Ti

The B–Ni–Ti system is only partially known: Kuzma and Chepiga [77] determined the 800 °C isothermal section excluding the B-rich corner, while, in the Ni-rich corner, the same isothermal section and the liquidus monovariant lines had been previously investigated by Schoebel and Stadelmaier [78]. Finally, a partial

Table 10
B–Hf–Ni invariant reactions involving liquid.

Invariant temperature (°C)	Reaction type[a]	Reaction
1741.5	*P*	Liquid + bcc-Hf + HfB ⇄ hcp-Hf
1199.6	*D*	Liquid + beta-$HfNi_3$ ⇄ alpha-$HfNi_3$, Hf_2Ni_7
1199.6	*D*	Liquid + beta-$HfNi_3$ ⇄ alpha-$HfNi_3$, Hf_8Ni_{21}
1174.9	*U*	Liquid + Hf_8Ni_{21} ⇄ alpha-$HfNi_3$ + Hf_3Ni_7
1150.0	*U*	Liquid + beta-HfNi ⇄ alpha-HfNi + Hf_9Ni_{11}
1150.0	*U*	Liquid + beta-HfNi ⇄ HfB_2 + alpha-HfNi
1150.0	*P*	Liquid + HfB_2 + beta-HfNi ⇄ alpha-HfNi
1150.0	*U*	Liquid + beta-HfNi ⇄ alpha-HfNi + Ni2B
1061.3	*U*	Liquid + HfB_2 ⇄ Ni_2B + NiB
1055.3	*E*	Liquid ⇄ $HfNi_5$ + $Hf_2Ni_{21}B_6$ + Hf_2Ni_7
1047.8	*E*	Liquid ⇄ $Hf_2Ni_{21}B_6$ + Ni + Ni_3B
1045.4	*E*	Liquid ⇄ Hf_2Ni + HfB + hcp-Hf
1038.5	*E*	Liquid ⇄ $HfNi_5$ + $Hf_2Ni_{21}B_6$ + Ni
1035.6	*U*	Liquid + alpha-HfNi ⇄ HfB_2 + Hf_9Ni_{11}
1032.9	*E*	Liquid ⇄ HfB_2 + $Hf_2Ni_{21}B_6$ + Ni_3B
1032.5	*E*	Liquid ⇄ HfB_2 + Ni_2B + Ni_3B
1032.4	*U*	Liquid + B ⇄ HfB_2 + NiB
1020.0	*E*	Liquid ⇄ HfB_2 + Ni_2B + o-Ni_4B_3
1019.5	*E*	Liquid ⇄ HfB_2 + m-Ni_4B_3 + o-Ni_4B_3
1017.1	*U*	Liquid + Hf_3Ni_7 ⇄ alpha-$HfNi_3$ + Hf_7Ni_{10}
1016.3	*E*	Liquid ⇄ HfB_2 + NiB + m-Ni_4B_3
1016.2	*E*	Liquid ⇄ HfB_2 + alpha-HfNi + Hf_2Ni
954.0	*U*	Liquid + Hf_9Ni_{11} ⇄ HfB_2 + Hf_7Ni_{10}
946.0	*E*	Liquid ⇄ HfB_2 + $Hf_2Ni_{21}B_6$ + Hf_2Ni_7
942.5	*U*	Liquid + Hf_2Ni_7 ⇄ HfB_2 + alpha-$HfNi_3$
864.7	*E*	Liquid ⇄ HfB_2 + alpha-$HfNi_3$ + Hf_7Ni_{10}

[a] *P* = ternary Peritectic, *U* = ternary transition (Übergang), *E* = ternary Eutectic, *D* = ternary Degenerate invariant equilibrium.

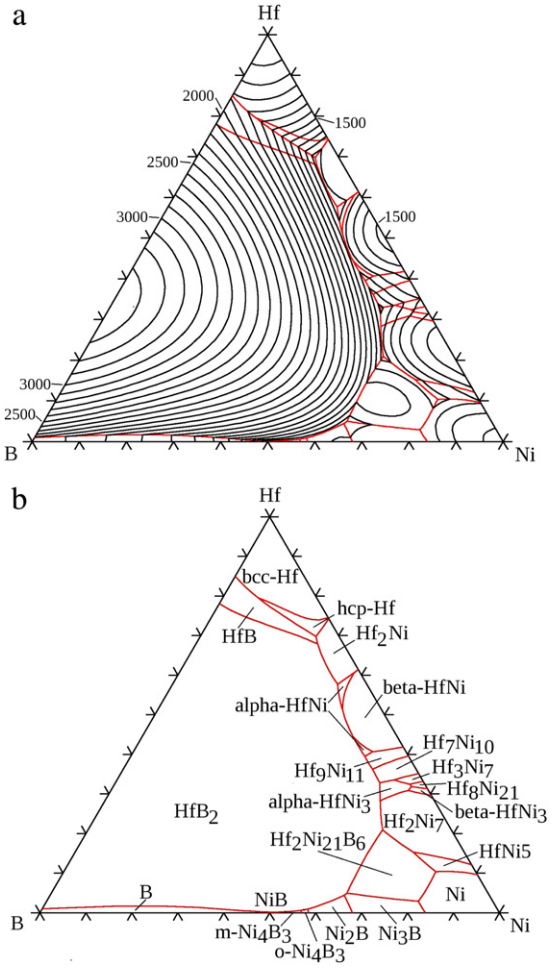

Fig. 12. The calculated B–Hf–Ni liquidus: (a) liquidus surface projection with isothermal lines (°C); (b) monovariant liquidus lines and primary solidification ranges.

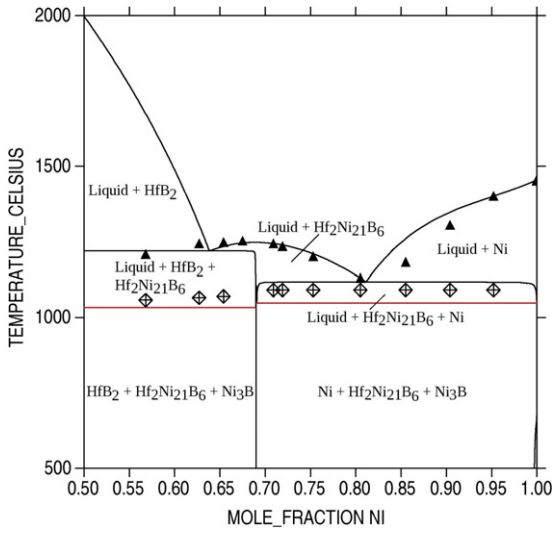

Fig. 13. The calculated B–Hf–Ni isopleth between $B_{0.668}Hf_{0.332}$ and pure Ni with liquidus (triangles) and sub-liquidus (diamonds) experimental points [73].

vertical section between pure Ni and the $Ti_2Ni_{21}B_6$ ternary compound was investigated by Lugscheider et al. [73]. Previous results by Samsonov [79] are considered not reliable because, while investigating the section between Ni and TiB_2, he did not detect the $Ti_2Ni_{21}B_6$ ternary compound.

No thermodynamic measurements nor CALPHAD assessments have been previously done for this system. B–Ni–Ti has then been assessed in this work by evaluating ternary parameters for the liquid phase and the only ternary compound $Ti_2Ni_{21}B_6$ on the basis of the available experimental data and the similarities with B–Hf–Ni. In this case too, $Ti_2Ni_{21}B_6$, isostructural with $Hf_2Ni_{21}B_6$, has been modelled as an ordered three-sublattice solid solution $(Ti\%, Ni)_3$ $(Ti, Ni\%)_{20}$ $(B)_6$ (see [76] and comments in the B–Hf–Ni section), but no mixing parameters have been introduced and the phase has been treated as stoichiometric at the $Ti_3Ni_{20}B_6$ composition.

Table 11
B–Ni–Ti invariant reactions involving liquid.

Invariant temperature (°C)	Reaction type[a]	Reaction
1092.6	*E*	Liquid ⇄ $TiB_2 + Ti_2Ni_{21}B_6 + Ni_3B$
1084.7	*E*	Liquid ⇄ $TiB_2 + Ni_2B + Ni_3B$
1051.0	*E*	Liquid ⇄ $Ti_2Ni_{21}B_6 + Ni + Ni_3B$
1032.9	*U*	Liquid + B ⇄ TiB_2 + NiB
1026.1	*E*	Liquid ⇄ $TiB_2 + Ni_2B$ + o-Ni_4B_3
1023.4	*E*	Liquid ⇄ TiB_2 + m-Ni_4B_3 + o-Ni_4B_3
1017.8	*E*	Liquid ⇄ TiB_2 + NiB + m-Ni_4B_3
1001.3	*E*	Liquid ⇄ $Ti_2Ni_{21}B_6 + Ni + TiNi_3$
983.4	*E*	Liquid ⇄ $TiB_2 + Ti_2Ni_{21}B_6 + TiNi_3$
967.6	*U*	Liquid + TiB_2 ⇄ TiNi + Ti_3B_4
939.4	*U*	Liquid + Ti_3B_4 ⇄ TiNi + TiB
865.6	*E*	Liquid ⇄ BCC_A2 + TiB + Ti_2Ni
861.9	*E*	Liquid ⇄ TiNi + TiB + Ti_2Ni
857.3	*E*	Liquid ⇄ TiB_2 + TiNi + $TiNi_3$

[a] *U* = ternary transition (Übergang), *E* = ternary Eutectic.

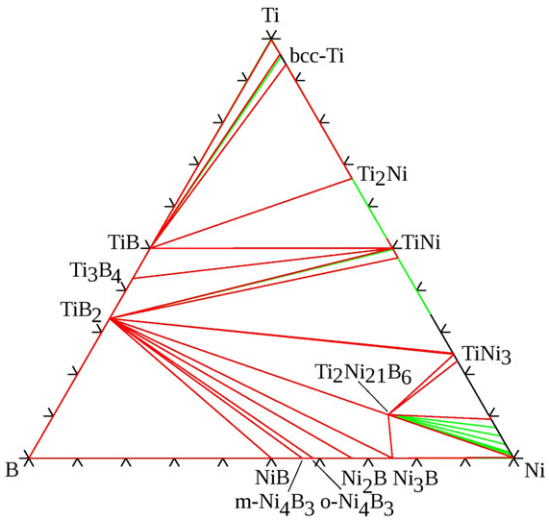

Fig. 14. The calculated B–Ni–Ti isothermal section at 800 °C.

The 800 °C isothermal section is reported in Fig. 14. A general good agreement with experiments is observed with a few discrepancies: (a) the Ti_3B_4 phase is missing in [77]; (b) the TiNi+TiB equilibrium results more stable than Ti_2Ni + TiB_2 reported by Kuzma and Chepiga [77]; (c) the composition of the fcc (Ni) phase in equilibrium with Ni_3B and $Ti_2Ni_{21}B_6$ is in agreement with [78], not with [77].

The projection of the liquidus surface with isothermal lines is reported in Fig. 15(a) while liquid monovariant lines are reported in Fig. 15(b) with indication of the primary solidification range for each phase. A reasonable agreement with experiments by Stadelmaier and Shoemaker [72] conducted in the Ni-rich corner and including the primary solidification range of $Ti_2Ni_{21}B_6$ has been obtained. Characteristic features of the projection are as follows: (a) the large primary solidification area of TiB_2 (which is however smaller than the HfB_2 area in B-Hf–Ni), (b) the deep valley close to the Ni–Ti binary subsystem which includes the lowest ternary eutectic of the system Liquid ⇄ TiB_2 + TiNi + $TiNi_3$ at 857 °C. All the invariant equilibria involving liquid are summarised in Table 11.

The isopleth between TiB_2 and Ni is shown in Fig. 16. There is fairly good agreement with experimental results by Lugscheider et al. [73] about the melting temperature of $Ti_2Ni_{21}B_6$ and the liquidus curve related to the Ni precipitation. However the experimental monovariant liquidus temperature between pure Ni and $Ti_2Ni_{21}B_6$ is lower than the computed one. A better agreement could subsist if the experimental temperature of 1088 °C could

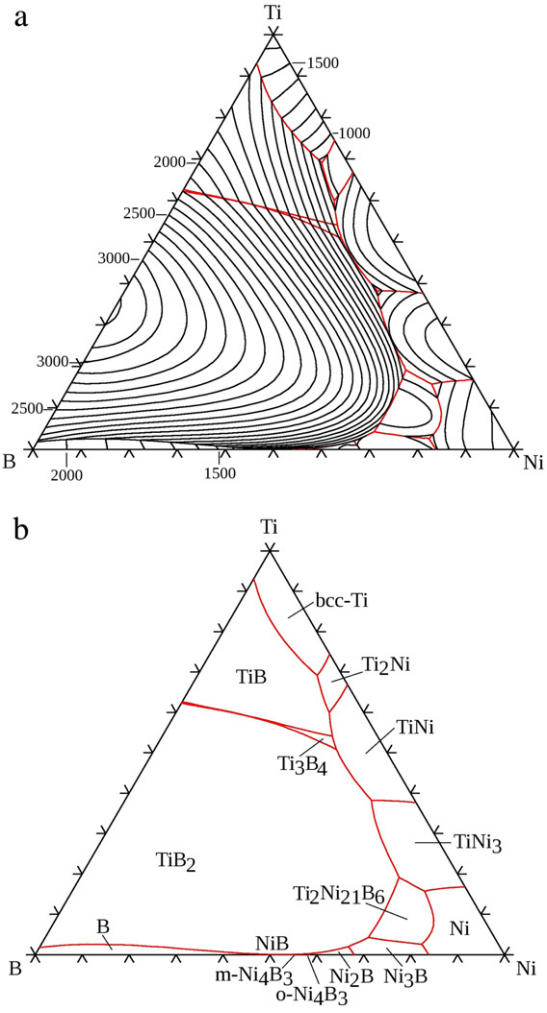

Fig. 15. The calculated B–Ni–Ti liquidus: (a) liquidus surface projection with isothermal lines (°C); (b) monovariant liquidus lines and primary solidification ranges.

be ascribed to the invariant equilibrium Liquid ⇄ $Ti_2Ni_{21}B_6$ + Ni + Ni_3B (notice that the three phase field Liquid + $Ti_2Ni_{21}B_6$ + Ni was not detected by Lugscheider et al. [73]). In general it was not possible to get a better agreement between computed and experimental liquidus: for instance, liquidus related to the TiB_2 precipitation seems to run at too high temperature. This may be an indication that the Redlich–Kister–Muggianu ternary parameters are unable to describe with good accuracy the liquid

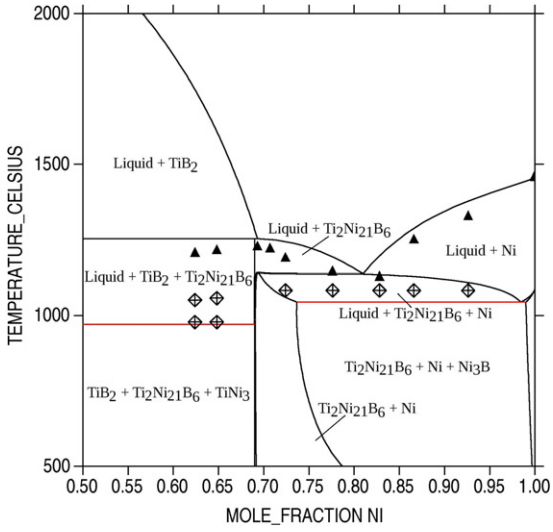

Fig. 16. The calculated B–Ni–Ti isopleth between $B_{0.666}Ti_{0.334}$ and pure Ni with liquidus (triangles) and sub-liquidus (diamonds) experimental points [73].

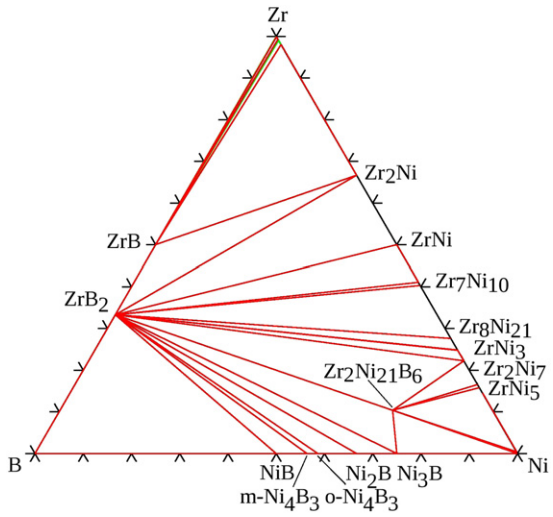

Fig. 17. The calculated B–Ni–Zr isothermal section at 850 °C.

thermodynamic functions in this system. However, due to lack of thermodynamic data on the liquid, it is not possible to introduce more sophisticated liquid models.

3.13. B–Ni–Zr

In the B–Ni–Zr system two isothermal sections have been investigated: by Voroshilov and Kuzma [80] at 850 °C in the whole composition range and by Stadelmaier and Helms [81] at 800 °C in the Ni-rich corner. Stadelmaier and Helms [81] also determined the liquidus monovariant lines in the same composition range, while [73] determined the partial vertical section between pure Ni and the $Zr_2Ni_{21}B_6$ ternary compound. No thermodynamic measurements nor CALPHAD assessments having been found in the literature B–Ni–Zr has been assessed in this work by evaluating ternary parameters for the liquid phase and the only ternary compound $Zr_2Ni_{21}B_6$ on the basis of the available experimental data and the similarities with B–Hf–Ni and B–Ni–Ti. In this case too, $Zr_2Ni_{21}B_6$, isostructural with $Hf_2Ni_{21}B_6$ and $Ti_2Ni_{21}B_6$, has been modelled as an ordered three-sublattice solid solution $(Zr\%, Ni)_3\ (Zr, Ni\%)_{20}\ (B)_6$ (see comments in the B–Hf–Ni section), but no mixing parameters have been introduced and the phase has been treated as stoichiometric at the $Zr_3Ni_{20}B_6$ composition.

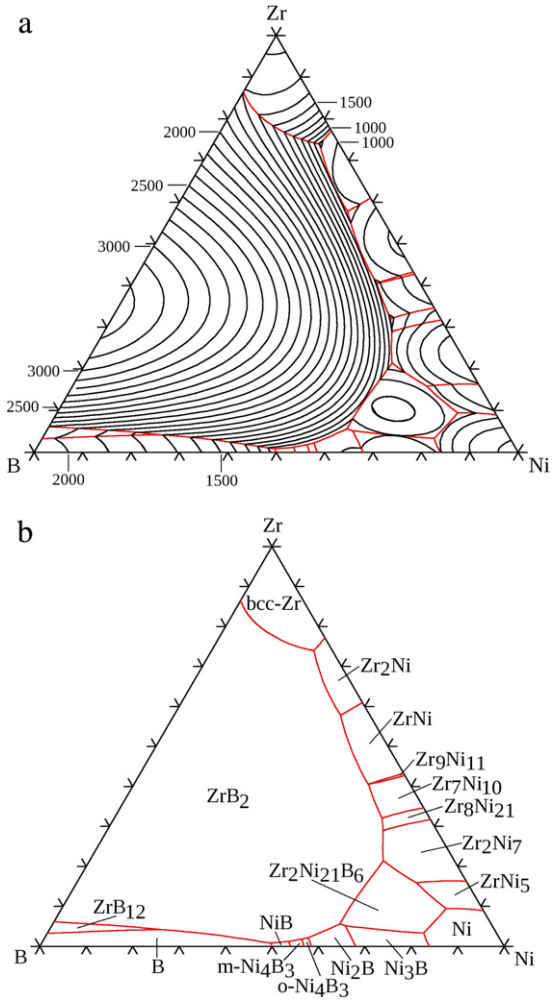

Fig. 18. The calculated B–Ni–Zr liquidus: (a) liquidus surface projection with isothermal lines (°C); (b) monovariant liquidus lines and primary solidification ranges.

The 850 °C isothermal section is reported in Fig. 17. A general good agreement with experiments is observed with a few exceptions: (a) o-Ni_4B_3 and m-Ni_4B_3 are not distinguished in [80]; (b) $ZrNi_3$ is missing in the [80] section; (c) according to [80] $Zr_2Ni_{21}B_6$ is in equilibrium with the Ni-rich Ni–Zr phases up to Zr_8Ni_{21} (identified as Zr_2Ni_5) while, according to the present assessment, it is in equilibrium with only $ZrNi_5$ and Zr_2Ni_7.

The projection of the liquidus surface with isothermal lines is reported in Fig. 18(a) while liquid monovariant lines are reported in Fig. 18(b) with indication of the primary solidification range for each phase. Calculated liquid monovariant lines are in reasonable agreement with experiments by Stadelmaier and Helms [81] in the Ni-rich corner of the system. Characteristic features of the projection are as follows: (a) the large primary solidification area of ZrB_2, (b) the deep valley close to the Zr–Ni binary subsystem which includes the lowest ternary eutectic of the system Liquid $\rightleftarrows ZrB_2 + Zr_7Ni_{10} + Zr_8Ni_{21}$ at 874 °C. All the invariant equilibria involving liquid are summarised in Table 12.

The isopleth between ZrB_2 and Ni is shown in Fig. 19. The computed liquidus curve is in partial agreement with experimental results by Lugscheider et al. [73]: there is good agreement about the liquidus curve related to the Ni precipitation and the monovariant liquidus temperature between pure Ni and $Ti_2Ni_{21}B_6$. However the melting temperature of $Ti_2Ni_{21}B_6$ seems slightly overestimated in the calculation.

Table 12
B–Ni–Zr invariant reactions involving liquid.

Invariant temperature (°C)	Reaction type[a]	Reaction
1706.0	*U*	Liquid + ZrB_{12} ⇄ ZrB_2 + B
1045.1	*E*	Liquid ⇄ $ZrNi_5$ + $Zr_2Ni_{21}B_6$ + Zr_2Ni_7
1034.8	*E*	Liquid ⇄ $Zr_2Ni_{21}B_6$ + Ni + Ni_3B
1026.9	*U*	Liquid + B ⇄ ZrB_2 + ZrNi
1019.1	*E*	Liquid ⇄ $ZrNi_5$ + $Zr_2Ni_{21}B_6$ + Ni
1007.8	*U*	Liquid + Ni_3B ⇄ $Zr_2Ni_{21}B_6$ + Ni_2B
1006.8	*E*	Liquid ⇄ ZrB_2 + ZrNi + m-Ni_4B_3
1003.9	*U*	Liquid + M_NI4B3 ⇄ ZrB_2 + o-Ni_4B_3
1000.3	*E*	Liquid ⇄ ZrB_2 + Ni_2B + o-Ni_4B_3
994.7	*E*	Liquid ⇄ ZrB_2 + bcc-Zr + Zr_2Ni
993.7	*E*	Liquid ⇄ ZrB_2 + $Zr_2Ni_{21}B_6$ + Zr_2Ni
977.8	*U*	Liquid + ZrNi ⇄ ZrB_2 + Zr_9Ni_{11}
977.2	*E*	Liquid ⇄ ZrB_2 + Zr_7Ni_{10} + Zr_9Ni_{11}
940.4	*E*	Liquid ⇄ ZrB_2 + ZrNi + Zr_2Ni
921.0	*E*	Liquid ⇄ ZrB_2 + $Zr_2Ni_{21}B_6$ + Zr_2Ni_7
874.5	*E*	Liquid ⇄ ZrB_2 + Zr_7Ni_{10} + Zr_8Ni_{21}

[a] *U* = ternary transition (Übergang), *E* = ternary Eutectic.

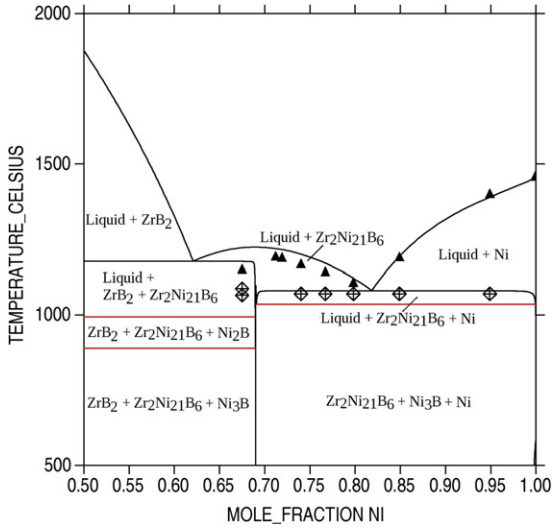

Fig. 19. The calculated B–Ni–Zr isopleth between $B_{0.668}Zr_{0.332}$ and pure Ni with liquidus (triangles) and sub-liquidus (diamonds) experimental points [73].

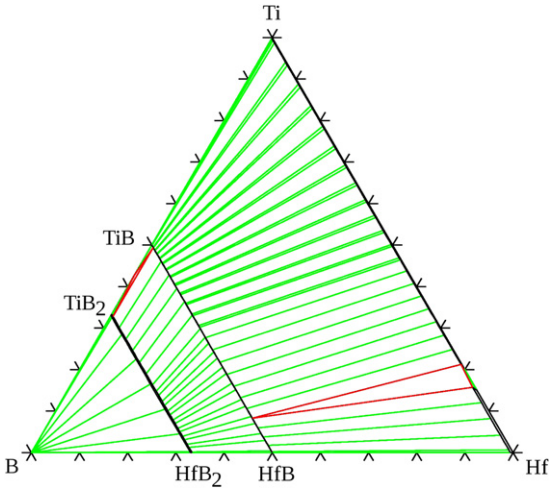

Fig. 20. The calculated B–Hf–Ti isothermal section at 1400 °C.

3.14. B–Hf–Ti

The B–Hf–Ti system was experimentally studied mainly by Chang [82] who investigated the following: (a) the complete solid solubility between the isostructural phases HfB_2 and TiB_2 as well as HfB and TiB; (b) the 1400 °C isothermal section between 0 and 67 at.% B; and (c) the liquidus surface in the whole composition range. Results from [82], together with a few more experimental data from different authors, are summarised and discussed by Bittermann and Rogl [24]. They also produced the only CALPHAD assessment available in the literature for this system: it has been adopted in this work.

The 1400 °C isothermal section, reported in Fig. 20, is in excellent agreement with the experiments by Chang [82]. Good agreement also subsist between the calculated (Fig. 21) and experimental liquidus projections. It may be noticed that no ternary invariant reactions involving liquid are present in this system.

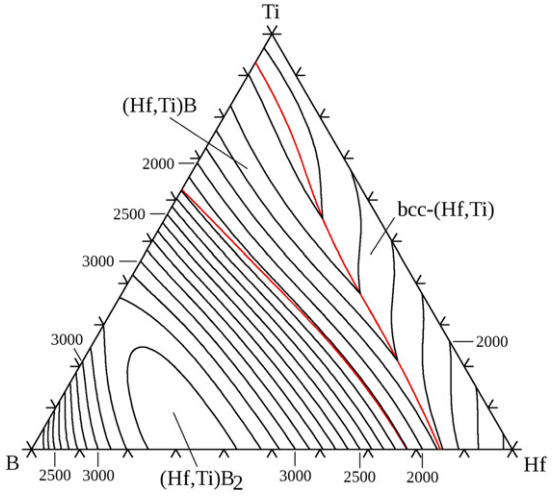

Fig. 21. The calculated B–Hf–Ti liquidus surface projection with isothermal lines (°C) and primary solidification ranges.

3.15. B–Hf–Zr

The B–Hf–Zr system has been investigated experimentally by Voroshilov and Kuzma [83] and Rudy [84]. The first one determined the isothermal section at 1500 °C, the second one investigated the isothermal section and 1775 °C and the liquidus projection in the complete composition range.

No experimental thermodynamics nor CALPHAD assessment is available in the literature for this system. It has then been

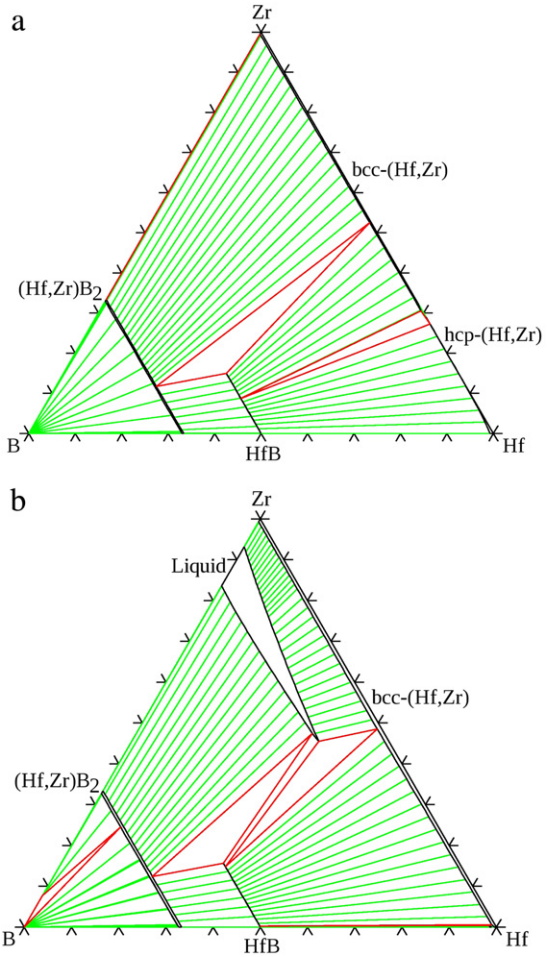

Fig. 22. The calculated B–Hf–Zr isothermal sections: (a) at 1500 °C; (b) at 1775 °C.

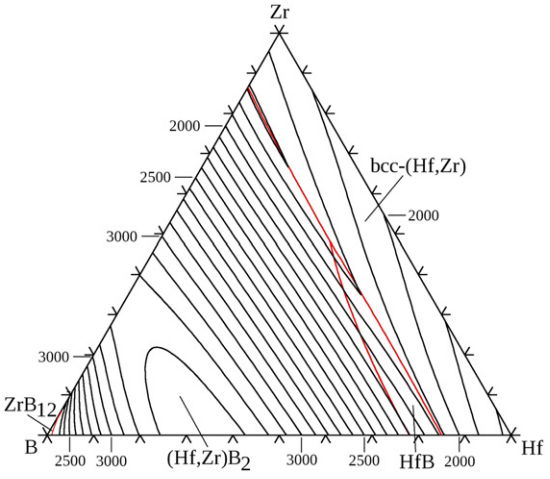

Fig. 23. The calculated B–Hf–Zr liquidus surface projection with isothermal lines (°C) and primary solidification ranges.

assessed in this work. The calculated isothermal sections at 1500 and 1775 °C, shown in Fig. 22, are in good agreement with experiments with the exception of the ternary solubility of HfB: very small according to [83] and substantial according to [84]. In this work agreement with [84] has been preferred. The computed liquidus surface projection is shown in Fig. 23. The only invariant equilibrium involving liquid is:
Liquid + HfB (Hf, Zr)B_2 + bcc-(Hf, Zr) calculated at 1763 °C and in reasonable agreement with the experimental temperature of 1715 °C.

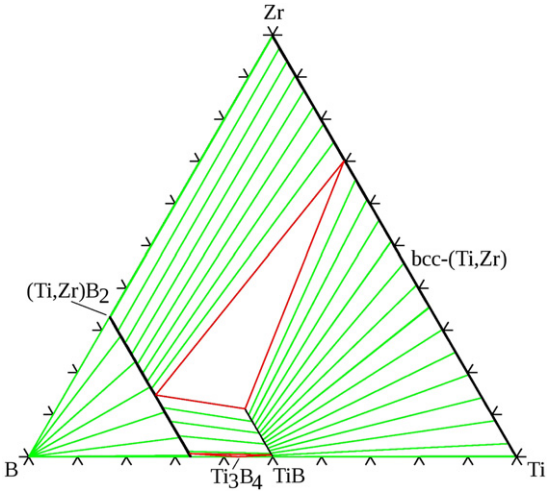

Fig. 24. The calculated B–Ti–Zr isothermal section at 1400 °C.

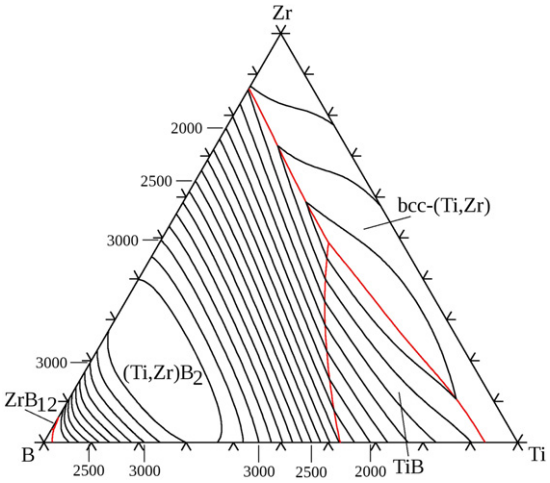

Fig. 25. The calculated B–Ti–Zr liquidus surface projection with isothermal lines (°C) and primary solidification ranges.

3.16. B–Ti–Zr

The B–Ti–Zr system has been investigated experimentally by Rudy [84] and Voroshilov and Kuzma et al. [83]. The first one determined the isothermal section at 1400 °C and the liquidus projection in the complete composition range while [83] investigated the isothermal section at 1500 °C. However he did not report the liquid phase, stable at this temperature according to [84].

No experimental thermodynamics nor CALPHAD assessment is available in the literature for this system, then it has been assessed in this work.

The calculated isothermal section at 1400 °C is shown in Fig. 24: it is in good agreement with experiments by Rudy [84]. The liquidus projection is reported in Fig. 25. In agreement with [84] there is a minimum in the monovariant liquidus curve liquid + TiB + (β-Ti) at about 1420 °C, in good agreement with an experimental value of 1445 °C. Two invariant equilibria involving liquid are present: Liquid + (Ti, Zr)B_2 $\rightleftarrows$ TiB + bcc-(Hf, Zr) calculated at 1424 °C, in reasonable agreement with the experimental temperature of 1450 °C, and Liquid + (Ti, Zr)B_2 $\rightleftarrows$ ZrB_{12} + B calculated at 2022 °C in excellent agreement with the experimental value of 2020 °C.

3.17. Hf–Ni–Ti

According to the critical assessment by Gupta [85] the only experimental investigation in the Hf–Ni–Ti system was carried out by Eremenko et al. [86]. They determined the vertical section at 50 at.% Ni where β-HfNi and NiTi, considered as isostructural

Table 13
Hf–Ni–Ti invariant reactions involving liquid.

Invariant temperature (°C)	Reaction type[a]	Reaction
1207.6	*E*	Liquid ⇄ $HfNi_5$ + Hf_2Ni_7 + Ni
1206.8	*U*	Liquid + Hf_9Ni_{11} ⇄ beta-HfNi + Hf_7Ni_{10}
1199.6	*U*	Liquid + beta-$HfNi_3$ ⇄ alpha-$HfNi_3$, Hf_8Ni_{21}
1199.6	*U*	Liquid+beta-$HfNi_3$ ⇄ alpha-$HfNi_3$, Hf_2Ni_7
1179.7	*E*	Liquid ⇄ Hf_2Ni_7 + Ni + $TiNi_3$
1174.9	*U*	Liquid + Hf_8Ni_{21} ⇄ alpha-$HfNi_3$ + Hf_3Ni_7
1113.7	*U*	Liquid + alpha-HfNi ⇄ beta-HfNi + Hf_2Ni
1090.2	*U*	Liquid + Hf_2Ni_7 ⇄ alpha-$HfNi_3$ + $TiNi_3$
1017.1	*U*	Liquid + Hf_3Ni_7 ⇄ alpha-$HfNi_3$ + Hf_7Ni_{10}
911.7	*U*	Liquid + alpha-$HfNi_3$ ⇄ Hf_7Ni_{10} + $TiNi_3$
892.3	*U*	Liquid + alpha-HfNi ⇄ bcc-(Hf, Ti) + beta-HfNi
889.1	*E*	Liquid ⇄ bcc-(Hf, Ti) + alpha-HfNi + Hf_2Ni
885.3	*U*	Liquid + TiNi ⇄ beta-HfNi + Ti_2Ni
882.6	*U*	Liquid + beta-HfNi ⇄ TiNi + Hf_7Ni_{10}
877.7	*E*	Liquid ⇄ TiNi + Hf_7Ni_{10} + $TiNi_3$
815.3	*E*	Liquid ⇄ bcc-(Hf, Ti) + beta-HfNi + Ti_2Ni

[a] *U* = ternary transition (Übergang), *E* = ternary Eutectic.

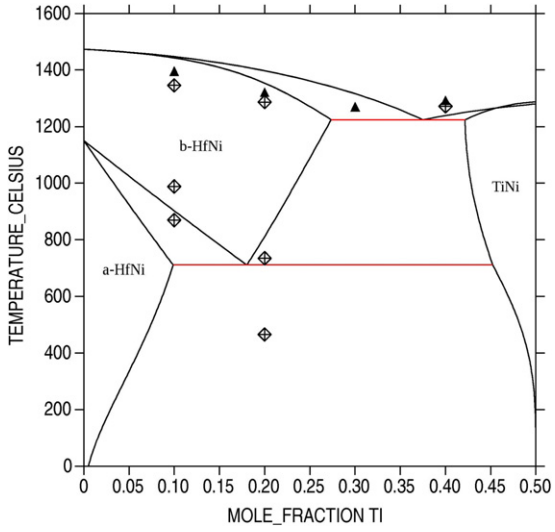

Fig. 26. The calculated Hf–Ni–Ti isopleth at 50 at.% Ni. Triangles and diamonds represent liquidus and sub-liquidus experimental curves by Eremenko and Semenova [86] quoted in [85].

phases, are reported to form a continuous solid solution with a minimum melting temperature of about 1260 °C at 30 at.% Ti. However it is still not clear whether β-HfNi and NiTi are isostructural phases and can form a continuous solid solution and, for this reason, they have been considered as separate phases in this work.

No CALPHAD assessment is available in the literature, the system has been assessed in this work with the only condition, taken from [86], that the liquidus in the HfNi–TiNi section has a minimum of about 1250 °C and 30 at.% Ti. The computed section is reported in Fig. 26: at temperatures higher than 800 °C it is in reasonable agreement with [86] with the obvious exception of the two-phase field β-HfNi + NiTi. However, due to the poor reliability of the solid state equilibria by Eremenko and Semenova [86] (for instance, they did not ascertain whether β-HfNi and NiTi are isostructural phases) they were not considered in the assessment.

The computed liquidus projection is shown in Fig. 27 and the invariant equilibria involving liquid are listed in Table 13.

3.18. Hf–Ni–Zr

According to the critical assessment by Gupta [87] the only experimental investigation in the Hf–Ni–Zr system was carried out by Eremenko et al. [86]. They determined the vertical section at 50 at.% Ni where the isostructural phases α-HfNi and ZrNi are reported to form a continuous solid solution while β-HfNi extends, at higher temperature, up to a few at.% from NiZr.

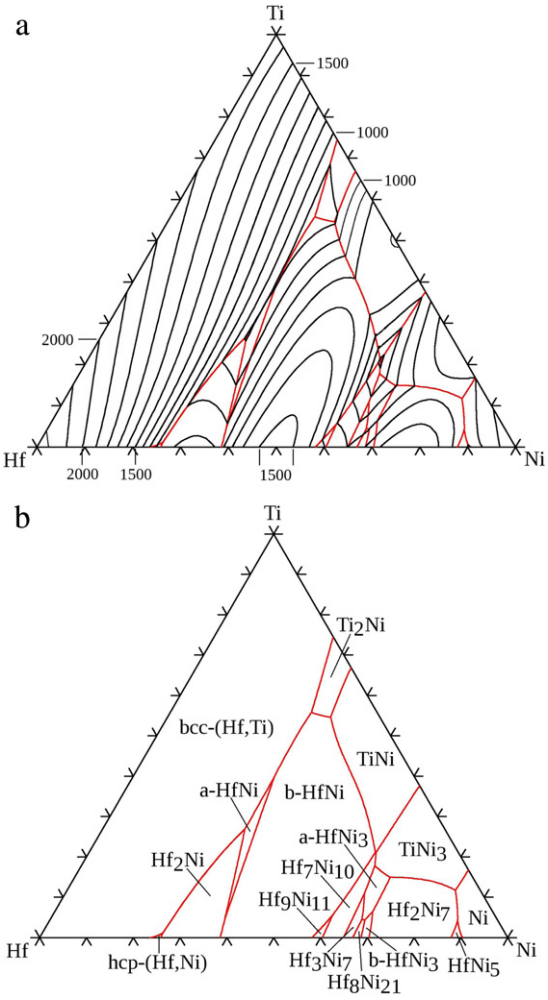

Fig. 27. The calculated Hf–Ni–Ti liquidus: (a) liquidus surface projection with isothermal lines (°C); (b) monovariant liquidus lines and primary solidification ranges.

No thermodynamic data nor CALPHAD assessments have been found in the literature for this system. In the CALPHAD assessment carried out in this work the vertical section reported by Eremenko and Semenova [86] has been taken into account with more attention to the liquidus curve, while other equilibria have been only qualitatively reproduced. The computed isopleth at 50 at.% Ni and the liquidus projection are shown in Figs. 28 and 29, respectively. Invariant equilibria involving liquid are listed in Table 14.

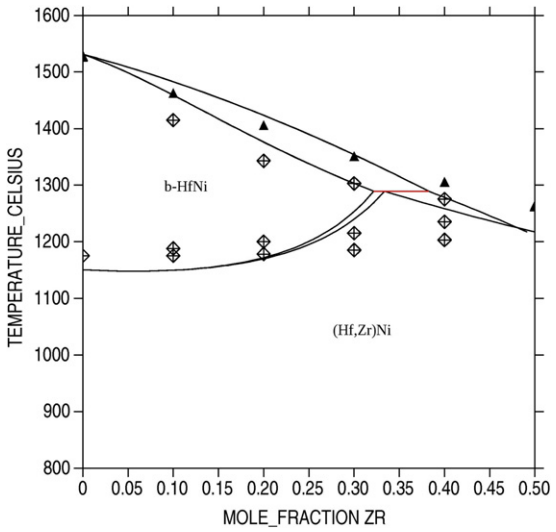

Fig. 28. The calculated Hf–Ni–Zr isopleth at 50 at.% Ni. Triangles and diamonds represent liquidus and sub-liquidus experimental curves by Eremenko and Semenova [86] quoted in [87].

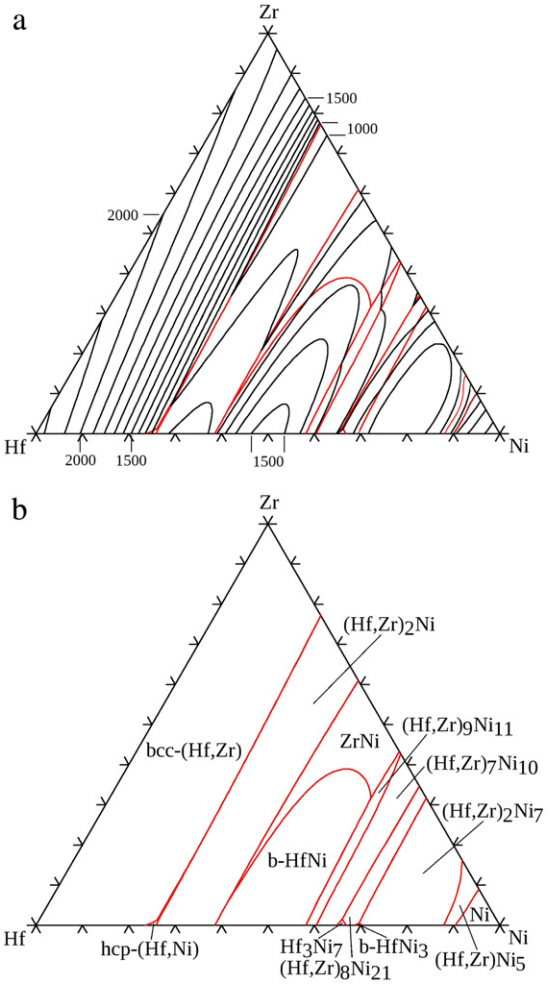

Fig. 29. The Hf–Ni–Zr liquidus: (a) liquidus surface projection with isothermal lines (°C); (b) monovariant liquidus lines and primary solidification ranges.

3.19. Hf–Ti–Zr

No literature data are available for the Hf–Ti–Zr system. Considering that these three elements belong to the same group and are chemically very similar to each other, an ideal ternary mixing behaviour has been assumed. A series of isothermal sections showing the variation with temperature of the hcp + bcc and bcc + liquid two-phase fields are reported in Figs. 30 and 31, respectively. Of course no invariant equilibrium is present in the system.

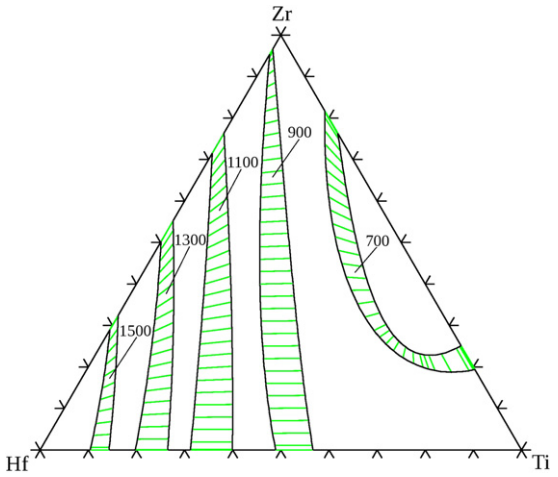

Fig. 30. Series of calculated Hf–Ti–Zr isothermal sections showing the variation with temperature (in °C) of the hcp + bcc two-phase field. For each temperature hcp is on the left and bcc on the right.

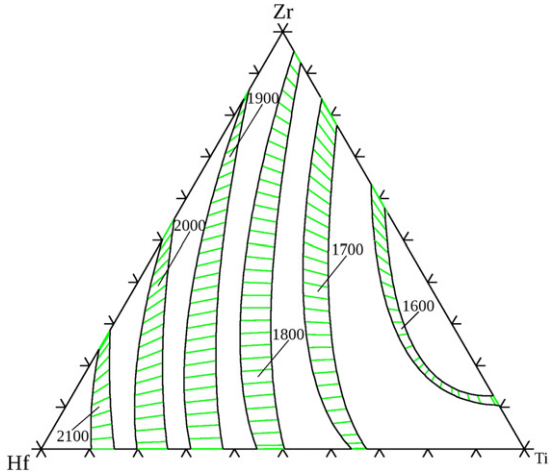

Fig. 31. Series of calculated Hf–Ti–Zr isothermal sections showing the variation with temperature (in °C) of the bcc + liquid two-phase field. For each temperature bcc is on the left and liquid on the right.

3.20. Ni–Ti–Zr

Ni–Ti–Zr phase diagram has been partially studied by Moloknov et al. [88], who investigated the Ti_2Ni–Zr_2Ni isopleth, and by Eremenko et al. [89–92,86] who investigated ternary phases, isopleths at 33 and 50 at.% Ni, liquidus projection, and the 700 °C isothermal section in the 0–50 at.% Ni composition range. A critical assessment of the system has been carried out by Gupta [93].

Two ternary phases have been identified in the system: τ_1, a $MgZn_2$ type Laves phase at 33 at.% Ni, and τ_2, a $BaPb_3$ type phase at 75 at.% Ni. No thermodynamic properties have been determined.

The Ni–Ti–Zr system has been modelled by Tokunaga et al. [94]. Their modelling, however, is not completely consistent with the present database. Then, starting from the [94] parameters, the system has been completely re-assessed obtaining not only a thermodynamic description consistent with the rest of the database, but also a better agreement with the experimental information. The τ_2 ternary phase, whose phase equilibria are completely unknown, has been omitted in the present assessment as well as in the previous one.

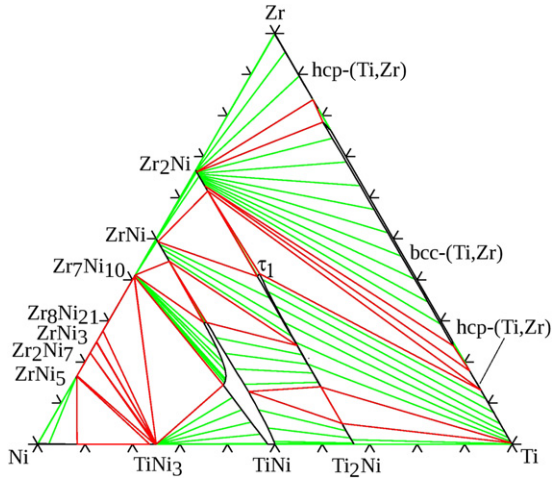

Fig. 32. The calculated Ni–Ti–Zr isothermal section at 700 °C.

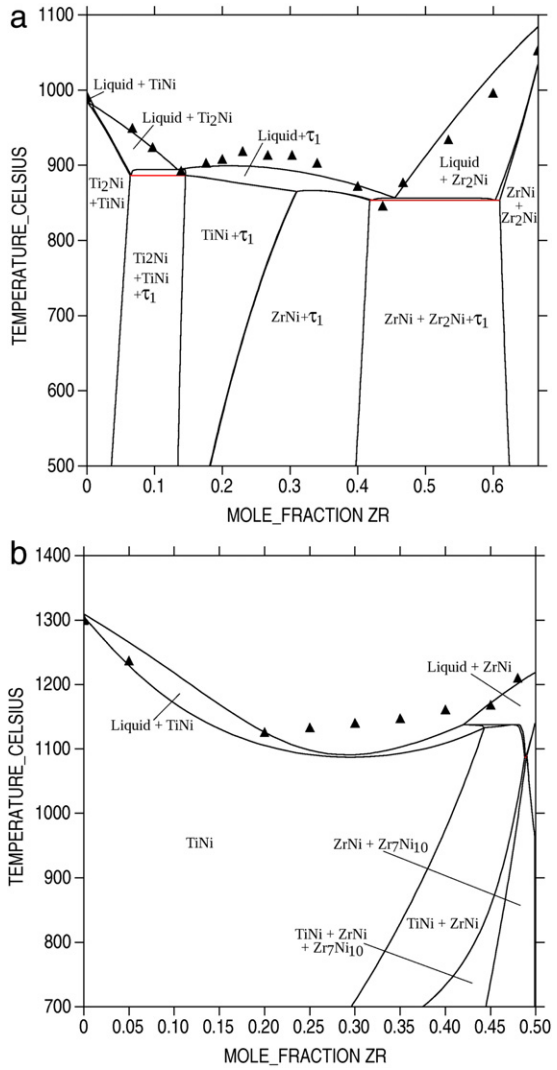

Fig. 33. The calculated Ni–Ti–Zr isopleths at (a) 33.4 at.% Ni with liquidus experimental points [86], and (b) 50.1 at.% Ni with liquidus experimental points [90].

Present results are summarised in Figs. 32–34 where the 700 °C isothermal section, the liquidus projection and the isopleths at 33 and 50 at.% Ni are reported, respectively. A general agreement with the experimental phase equilibria may be observed, especially for equilibria involving the liquid phase. The most remarkable

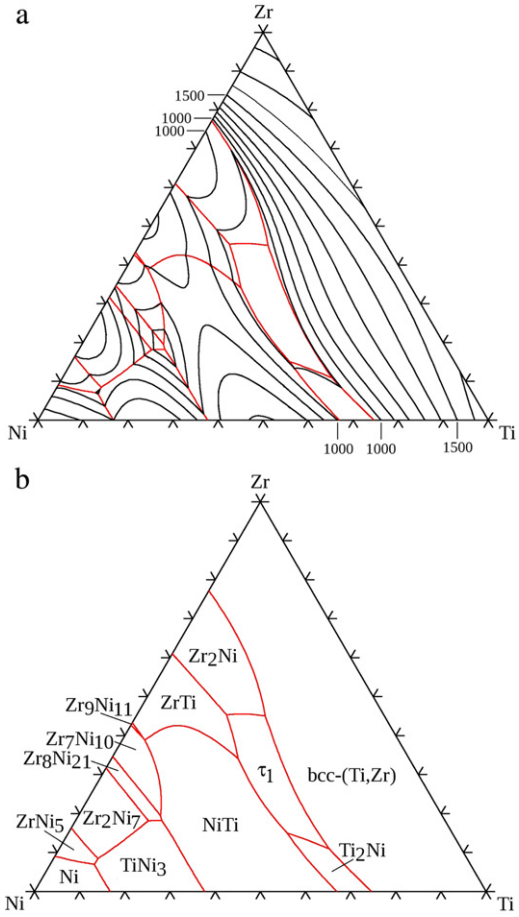

Fig. 34. The calculated Ni–Ti–Zr liquidus: (a) liquidus surface projection with isothermal lines (°C); (b) monovariant liquidus lines and primary solidification ranges.

discrepancy may be noted in the 700 °C isothermal section (Fig. 32) where the Ti–Zr phase in equilibrium with Zr_2Ni and τ_1 is hcp-(Ti,Zr) at about 15 at.% Zr instead of bcc–(Ti,Zr) at about 70 at.% Zr as determined by Eremenko et al. [89].

Invariant equilibria involving liquid calculated in this work are presented and listed in Table 15.

4. Conclusions

A CALPHAD thermodynamic database for phase diagram calculations in the quinary system B–Hf–Ni–Ti–Zr has been implemented. Thermodynamic models for 30 different phases have been determined and interaction parameters for all the 10 binary and 10 ternary sub-systems have been included. Interaction parameters have been taken from the literature, when available, but a few binary systems (B–Hf, B–Ti, B–Zr, Hf–Ni, Ni–Zr) have been slightly modified with respect to the previous assessments and several ternary systems (B–Hf–Ni, B–Ni–Ti, B–Ni–Zr, B–Hf–Zr, B–Ti–Zr, Hf–Ni–Ti, Hf–Ni–Zr, Hf–Ti–Zr, Ni–Ti–Zr) have been completely assessed or re-assessed in this work with particular attention to the self-consistency of the models adopted.

Assuming that higher order interactions may be approximated by ideal extrapolation of binary and ternary terms, quaternary and higher order equilibria may be predicted. Prediction of phase equilibria in higher order systems not investigated experimentally is further supported by a careful self-consistency check of the phase modelling and interaction parameters adopted from the literature or evaluated in this work.

The database has been especially built for application to the investigation of the interactions between Group 4 metal diboride UHTC and nickel, especially to predict and/or understand phase

Table 14
Hf–Ni–Zr invariant reactions involving liquid.

Invariant temperature (°C)	Reaction type[a]	Reaction
1230.3	*U*	Liquid + beta-HfNi ⇄ (Hf, Zr)Ni + (Hf, Zr)$_9$Ni$_{11}$
1184.4	*E*	Liquid ⇄ (Hf, Zr)$_7$Ni$_{10}$ + (Hf, Zr)$_8$Ni$_{21}$ + Hf$_3$Ni$_7$
1148.3	*U*	Liquid + (Hf, Zr)Ni ⇄ beta-HfNi + (Hf, Zr)$_2$Ni
1047.9	*U*	Liquid + hcp-(Hf, Zr) ⇄ bcc-(Hf, Zr) + (Hf, Zr)$_2$Ni

[a] *U* = ternary transition (Übergang), *E* = ternary Eutectic.

Table 15
Ni–Ti–Zr invariant reactions involving liquid.

Invariant temperature (°C)	Reaction type[a]	Reaction
1103.2	*U*	Liquid + Zr$_2$Ni$_7$ ⇄ ZrNi$_5$ + TiNi$_3$
1090.3	*E*	Liquid ⇄ ZrNi$_5$ + Ni + TiNi$_3$
1089.9	*U*	Liquid + Zr$_9$Ni$_{11}$ ⇄ ZrNi + Zr$_7$Ni$_{10}$
1086.7	*U*	Liquid + ZrNi ⇄ TiNi + Zr$_7$Ni$_{10}$
886.4	*U*	Liquid + Ti$_2$Ni ⇄ TiNi + τ_1
865.3	*E*	Liquid ⇄ TiNi + ZrNi + τ_1
853.5	*E*	Liquid ⇄ ZrNi + Zr$_2$Ni + τ_1
818.5	*U*	Liquid + Zr$_7$Ni$_{10}$ ⇄ TiNi + Zr$_8$Ni$_{21}$
816.9	*E*	Liquid ⇄ bcc-(Ti, Zr) + Zr$_2$Ni + τ_1
811.4	*E*	Liquid ⇄ TiNi + Zr$_8$Ni$_{21}$ + TiNi$_3$

[a] *U* = ternary transition (Übergang), *E* = ternary Eutectic.

Table A.1
List of the solid phases modelled in the B–Hf–Ni–Ti–Zr database. For each sublattice, the main constituents are in bold. Symbol VA represents vacancies (vacuum).

N	*Phase name*	*Structure (Pearson symbol, prototype, strukturbericht)*	*Formulae*	*Sublattice model*
1	FCC_A1	cF4, Cu, A1	Ni	(Hf, **Ni**, **Ti**, Zr$_1$ (B, **VA**)$_1$
2	BCC_A2	cI2, W, A2	beta-Hf, beta-Ti, beta-Zr	(**Hf**, Ni, **Ti**, **Zr**, VA)$_1$ (B, **VA**)$_3$
3	HCP_A3	hP2, Mg, A3	alpha-Hf, alpha-Ti, alpha-Zr	(**Hf**, Ni, **Ti**, **Zr**)$_1$ (B, **VA**)$_{0.5}$
4	BETA_B	rP105,	beta-B	(B)$_1$
5	TI3B4	oI14, Ta$_3$B$_4$, D7$_n$	Ti$_3$B$_4$	(Ti)$_3$ (B)$_4$
6	ZRB12	cF52, UB$_{12}$, D2$_f$	ZrB$_{12}$	(Zr)$_1$ (B)$_{12}$
7	ZRB	cF8, NaCl, B1	ZrB	(Zr)$_1$ (B)$_1$
8	M-NI4B3	mC*,,	m–Ni$_4$B$_3$	(Ni)$_{0.564}$ (B)$_{0.436}$
9	O-NI4B3	oP*,,	o–Ni$_4$B$_3$	(Ni)$_{0.586}$ (B)$_{0.414}$
10	NI3B	oP16, Fe$_3$C, D0$_{11}$	Ni$_3$B	(Ni)$_{0.75}$ (B)$_{0.25}$
11	HF3NI7		Hf$_3$Ni$_7$	(Hf)$_3$ (Ni)$_7$
12	A_HFNI3	hR12, BaPb$_3$,	alpha-HfNi$_3$	(Hf)$_1$ (Ni)$_3$
13	B_HFNI3	hP40,,	beta-HfNi$_3$	(Hf)$_1$ (Ni)$_3$
14	ALB2_TY	hP3, AlB$_2$, C32	HfB$_2$, TiB$_2$, ZrB$_2$	(**Hf**, **Ti**, VA, **Zr**)$_1$ (B)$_2$
15	FEB_TY	oP8, FeB, B27	HfB,TiB,	(**Hf**, **Ti**, VA, **Zr**)$_1$ (B)$_1$
16	CRB_TY	oC8, CrB, B$_f$	ZrNi, NiB, alpha-HfNi	(Ni)$_1$ (**B**, **Hf**, Ti, **Zr**)$_1$
17	B_HFNI		beta-HfNi	(**Hf**, Ti, Zr)$_1$ (Ni)$_1$
18	ET9NI11	tI40,,	Zr$_9$Ni$_{11}$, Hf$_9$Ni$_{11}$	(Hf, Zr)$_9$ (Ni)$_{11}$
19	ET8NI21	aP29,,	Zr$_8$Ni$_{21}$	(Hf, Zr)$_8$ (Ni)$_{21}$
20	ET2NI7	mC36,,	Zr$_2$Ni$_7$, Hf$_2$Ni$_7$	(Hf, Zr)$_2$ (Ni)$_7$
21	CUAL2_TY	tI12, Al$_2$Cu, C16	Zr$_2$Ni, Ni$_2$B, Hf$_2$Ni	(**Hf**, **Ni**, Ti, **Zr**)$_2$ (**B**, **Ni**, VA)
22	TI2NI	cF96,,	Ti$_2$Ni	(Ni, **Ti**, Zr)$_2$ (**Ni**, Ti)$_1$
23	MGZN2_TY	hP12, MgZn$_2$, C14	τ_1	(Ni, **Ti**, **Zr**)$_2$ (**Ni**, Ti, Zr)$_1$
24	ET7NI10	oC68,,	Zr$_7$Ni$_{10}$, Hf$_7$Ni$_{10}$	(**Hf**, VA, **Zr**)$_7$ (**Ni**, Zr)$_{10}$
25	NI3ZR1	hP8, Ni$_3$Sn, D0$_{19}$	ZrNi$_3$	(Ni, Zr)$_{0.75}$ (VA, Zr)$_{0.25}$
26	AUBE5_TY	cF24, AuBe$_5$, C15$_b$	ZrNi$_5$, HfNi$_5$	(**Hf**, **Zr**, VA)$_1$ (**Ni**, Zr)$_5$
27	NI3TI	hP16, TiNi$_3$, D0$_{24}$	TiNi$_3$	(**Ni**, Ti)$_3$ (Ni, **Ti**)$_1$
28	CR23C6_TY	cF116, Cr$_{23}$C$_6$	Zr$_2$Ni$_{21}$B$_6$, Ti$_2$Ni$_{21}$B$_6$, Hf$_2$Ni$_{21}$B$_6$	(**Hf**, Ni,**Ti**, **Zr**)$_3$ (Hf, **Ni**, Ti, Zr)$_{20}$ (B)$_6$
29	FCC2	cP4, AuCu$_3$, L1$_2$	Metastable TiNi$_3$	(Hf, **Ni**, Ti, Zr)$_{0.75}$ (Hf, Ni, **Ti**, Zr)$_{0.25}$ (VA)$_1$
30	BCC2	cP2, CsCl, B2	TiNi	(Hf, **Ni**, Ti, VA, Zr)$_{0.5}$ (Hf, Ni, **Ti**, VA, Zr)$_{0.5}$ (VA)$_3$

interactions in wetting experiments conducted on metal diboride surfaces. However, it may be used for calculations in the entire B–Hf–Ni–Ti–Zr quinary system.

HfB_2, TiB_2 and ZrB_2 samples usually include an appreciable amount of silicon derived from silicon nitride or carbide used as sintering aid during metal diboride synthesis. Then, to improve the predictive ability of the database when applied to the study of the Group 4 diboride-metal interactions, Si should be added. This is in progress and will be presented in a future paper.

Acknowledgements

This work has been carried out in the framework of a cooperation between "Dipartimento di Chimica e Chimica Industriale – Università di Genova" and "Istituto per l'Energetica e le Interfasi – IENI CNR".

Drs. A. Passerone and M.L. Muolo of the "Istituto per l'Energetica e le Interfasi — IENI CNR" are acknowledged with thanks for inspiration and interesting discussions about the subject of the present paper.

Appendix A. Table solid phases

See Table A.1.

Appendix B. Supplementary data

Supplementary material related to this article can be found online at doi:10.1016/j.calphad.2011.10.003.

References

[1] R.G. Munro, J. Res. NIST 105 (2000) 709–720.
[2] W.G. Fahrenholtz, G.E. Hilmas, I.G. Talmy, J.A. Zaykoski, J. Am. Ceram. Soc. 90 (2007) 1347–1364.
[3] M.M. Opeka, I.G. Talmy, J.A. Zaykoski, J. Mater. Sci. 39 (2004) 5887.
[4] D.M. Van Wie, D.G. Drewry Jr., D.E. King, C.M. Hudson, J. Mater. Sci. 39 (2004) 5915.
[5] J.P. Bonal, A. Kohyama, J. Van der Laan, L.L. Snead, MRS Bull. 34 (2009) 28–34.
[6] L. Giancarli, J.P. Bonal, A. Caso, G. Le Marois, N.B. Morly, J.F. Salavy, Fusion Eng. Design 41 (1998) 165–171.
[7] K. Kuwabara, S. Sakamoto, O. Kida, T. Ishino, T. Kodama, H. Nakajima, T. Ito, Y. Hirakawa, K. Asano (Eds.) The Proceedings of UNITECR 2003, Osaka, Technical Association of Refractories, 2003.
[8] A.M. Weimer, Carbide, Nitride and Boride Materials, Synthesis and Processing, Chapman & Hall, 1997.
[9] Z.J. Jin, M. Zhang, D.M. Guo, R.K. Kang, Key Eng. Mater. 291–292 (2005) 537.
[10] J. Sung, D.M. Goedde, G.S. Girolami, J.R. Abelson, J. Appl. Phys. 91 (2002) 3904.
[11] Y. Murata, US Patent 3 (1970) 487–594.
[12] M.L. Muolo, E. Ferrera, R. Novakovic, A. Passerone, Scr. Mater. 48 (2003) 191–196.
[13] M.L. Muolo, E. Ferrera, A. Passerone, J. Mater. Sci. 40 (2005) 2295.
[14] A. Passerone, M.L. Muolo, D. Passerone, J. Mater. Sci. 41 (2006) 5088.
[15] L. Kaufman, G. Cacciamani, M.L. Muolo, F. Valenza, A. Passerone, CALPHAD 34 (2010) 2–5.
[16] A. Passerone, M.L. Muolo, F. Valenza, L. Kaufman, CALPHAD 34 (2010) 6–14.
[17] A.T. Dinsdale, SGTE PURE4 database, ver. 4.6, 2008, www.sgte.org.
[18] G. Inden, Project Meeting CALPHAD V Symp Proceeding, 1976, vol. III, pp. 4–11.
[19] G. Inden, Physica B 103 (1981) 82.
[20] M. Hillert, M. Jarl, CALPHAD 2 (1978) 227.
[21] E. Rudy, S. Windisch, Tech. report AFML-TR-65-2, Part 1, vol. IX, Air Force Mat. Lab., Wright-Patterson A.F. Base, Ohaio, 1965.
[22] K.I. Portnoi, I.V. Romanovich, Y.V. Levinskii, S.A. Prokof'ev, Inorg. Mater. 7 (1972) 1769–1772.
[23] H. Okamoto, in: T.B. Massalski (Ed.), Binary Alloy Phase Diagrams, second ed., ASM International, 1990.
[24] H. Bittermann, P. Rogl, J. Phase Equilib. 18 (1997) 24–47.
[25] P. Rogl, P.E. Potter, CALPHAD 12 (1988) 207–218.
[26] P.K. Liao, K.E. Spear, in: P. Nash (Ed.), Phase Diagrams of Binary Nickel Alloys, ASM, 1991.
[27] W.-H. Sun, Y. Du, Y. Kong, H.-H. Xu, W. Xiong, S.-H. Liu, J. Mater. Res. 100 (2009) 59–67.
[28] K. Hack, T.G. Chart, CECA 7210-CA/3/303, Comm. Comun. Europ., 1980.
[29] O. Teppo, P. Taskinen, Mater. Sci. Technol. 93 (1993) 205–212.
[30] C.E. Campbell, U.R. Kattner, J. Phase Equilib. 20 (1999) 485–496.
[31] J.L. Murray, P.K. Liao, K.E. Spear, Bull. Alloy Phase Diagrams 7 (1986) 550–555.
[32] V.T. Witusiewicz, A.A. Bondar, U. Hecht, S. Rex, T.Ya. Velikanova, J. Alloys Compounds 448 (2008) 185–194.
[33] A. Jain, R. Pankajavalli, S. Anthonysamy, K. Ananthasivan, R. Babu, V. Ganesan, G.S. Gupta, J. Alloys Compounds 491 (2010) 747–752.
[34] C. Baetzner, Ph.D. Thesis, University of Stuttgart, Germany, 1994.
[35] X. Ma, C. Li, Z. Du, W. Zhang, J. Alloys Compounds 370 (2004) 149–158.
[36] H. Okamoto, J. Phase Equilib. 14 (1993) 261–262.
[37] F.W. Glazer, B. Post, Trans. AIME 197 (1953) 1117–1118.
[38] H. Nowotny, E. Rudy, F. Benesovsky, Monatsh. Chem. 91 (1960) 963–974.
[39] O.I. Shulishova, I.A. Shcherbak, Inorg. Mater. 3 (1967) 1304–1306.
[40] T. Tokunaga, K. Terashima, H. Ohtani, M. Hasebe, Mater. Trans. 49 (2008) 2534–2540.
[41] H. Duschanek, in: P. Rogl (Ed.), Phase Diagrams of Ternary Metal–Boron–Carbon Systems, ASM, 1998.
[42] H.M. Chen, F. Zheng, H.S. Liu, L.B. Liu, Z.P. Jin, J. Alloys Compounds 468 (2009) 209–216.
[43] P. Nash, A. Nash, Bull. Alloy Phase Diagrams 4 (1983) 250–253.
[44] V.N. Svechnikov, A.K. Shurin, G.P. Dmitriyeva, Izv. Akad. Nauk SSSR Met. (1967) 176–179.
[45] L. Bsenko, J. Less-Common Met. 63 (1979) 171–179.
[46] V.N. Yeremenko, E.L. Semenova, L.A. Tretyachenko, V.M. Petyukh, J. Alloys Compounds 191 (1993) 117–119.
[47] H. Okamoto, J. Phase Equilib. 14 (1993) 769.
[48] N. Selhaoui, J.-C. Gachon, J. Hertz, Metall. Trans. B 23 (1992) 815–819.
[49] L. Bencze, K. Hilpert, Metall. Mater. Trans. A 27 (1996) 3576–3590.
[50] Q. Guo, O.J. Kleppa, J. Alloys Compounds 269 (1998) 181–186.
[51] K.J. Zeng, Z.P. Jin, J. Less-Common Met. 166 (1990) 21–27.
[52] T. Wang, Z. Jin, J.-C. Zhao, Z. Metallkunde 92 (2001) 441–446.
[53] J.L. Murray, Bull. Alloy Phase Diagrams 2 (1981) 181–185.
[54] J.P. Abriata, J.C. Bolcich, H.A. Peretti, Bull. Alloy Phase Diagrams 3 (1982) 29–34.
[55] H. Bittermann, P. Rogl, J. Phase Equilib. 23 (2002) 218–235.
[56] J.L. Murray, in: P. Nash (Ed.), Phase Diagrams of Binary Nickel Alloys, ASM International, 1991.
[57] R. Lück, B. Arpshofen, I. Predel, J.F. Smith, Thermochim. Acta 131 (1988) 171–181.
[58] U. Thiedemann, M. Rosner-Kuhn, K. Drewes, G. Kuppermann, M.G. Frohberg, J. Non-Cryst. Solids 250 (1999) 329–335.
[59] P. Bellen, K.C. Hari Kumar, P. Wollants, Z. Metallkde. 87 (1996) 972–978.
[60] W. Tang, B. Sundman, R. Sandström, C. Qiu, Acta Mater. 47 (1999) 3457–3468.
[61] T. Tokunaga, K. Hashima, H. Ohtani, M. Hasebe, Mater. Trans. 45 (2004) 1507–1514.
[62] J. De Keyzer, G. Cacciamani, N. Dupin, P. Wollants, CALPHAD 33 (2009) 109–123.
[63] P. Nash, C.S. Jayanth, Bull. Alloy Phase Diagrams 5 (1984) 144–148.
[64] F.N. Wang, C. Li, Z. Du, J. Li, F. Wang, F. Wang, Int. J. Mater. Res. 2008/07 (2008) 712–715.
[65] G. Ghosh, J. Mater. Res. 9 (1994) 598–616.
[66] T. Tokunaga, S. Matsumoto, H. Ohtani, M. Hasebe, J. Japan Inst. Metals 70 (2006) 741–749.
[67] J.L. Murray, in: J.L. Murray (Ed.), Phase Diagrams of binary Titanium Alloys, ASM International, 1987, pp. 340–345.
[68] U. Thiedemann, M. Rosner-Kuhn, K. Drewes, G. Kuppermann, M.G. Frohberg, Steel Res. 70 (1999) 3–8.
[69] K.C. Hari Kumar, P. Wollants, L. Delaey, J. Alloys Compounds 206 (1994) 121–127.
[70] M.A. Turchanin, P.G. Agraval, A.R. Abdulov, Powder Metall Metal Ceramics 47 (2008) 428–446.
[71] Y.B. Kuzma, Visnik L'Vivs'Kogo Derez. Univ., Ser. Khimichna 14 (1972) 20–25.
[72] H.H. Stadelmaier, C.A. Shoemaker, Metall 20 (1966) 1056–1057.
[73] E. Lugscheider, H. Reimann, R. Pankert, Metall 36 (1982) 247–251.
[74] L. Kaufman, G. Cacciamani, M.L. Muolo, F. Valenza, A. Passerone, CALPHAD 34 (2010) 2–5.
[75] A. Passerone, M.L. Muolo, F. Valenza, L. Kaufman, CALPHAD 34 (2010) 6–14.
[76] E. Ganglberger, H. Nowotny, F. benesovsky, Monatsch. Chemie. 96 (1965) 1144–1146.
[77] Y.B. Kuzma, M.V. Chepiga, Soviet Powder Metall Metal Ceramics 8 (1969) 832–835.
[78] J.D. Schoebel, H.H. Stadelmaier, Metall 19 (1965) 715–717.
[79] G.V. Samsonov, Metalloved. Term. Obrab. Met. 1 (1958) 35–38.
[80] J.V. Voroshilov, J.B. Kuzma, Visnik L'Viv'kogo Derz. Univ., Ser. Khim. 9 (1967) 17–20.
[81] H.H. Stadelmaier, B.B. Helms, Metall 19 (1965) 121–122.
[82] Y.A. Chang, Tech. report AFML-TR-65-2, Part 2, vol. V, Ohaio, 1966.
[83] Yu.V. Voroshilov, Yu.B. Kuzma, Soviet Powder Metall Metal Ceramics 8 (1969) 941–944.
[84] E. Rudy, Tech. report AFML-TR-65-2, Part 5, AD 689843, Air Force Mat. Lab., Wright-Patterson A.F. Base, Ohaio, 1969.
[85] K.P. Gupta, J. Phase Equilib. 22 (2001) 69–72.
[86] N.N. Eremenko, E.L. Semenova, L.A. Tretyachenko, V.M. Petyukh, Russ. Akad. Nauk Neorg. Mater. 28 (1992) 1173–1177.
[87] K.P. Gupta, J. Phase Equilib. 22 (2001) 73–77.
[88] V.V. Moloknov, V.N. Chebotnikov, V.V. Molokanov, Yu.K. Koveneristyi, Izv. Akad. Nauk SSSR Neorganic. Mater. 25 (1989) 61–65.
[89] V.N. Eremenko, E.L. Semenova, L.A. Tretyachenko, Dop. Akad. Nauk Ukr. RSR Fiz. Met. Tekh. (1988) 76–79.
[90] V.N. Eremenko, E.L. Semenova, L.A. Tretyachenko, Izv. V.U.Z. Tsvetn. Metall (1990) 85–88.
[91] V.N. Eremenko, E.L. Semenova, L.A. Tretyachenko, Poroshk. Metall (1991) 49–54.
[92] V.N. Eremenko, E.L. Semenova, L.A. Tretyachenko, Dokl. Akad. Nauk SSSR Metall (1991) 191–196.
[93] K.P. Gupta, J. Phase Equilib. (1999) 441–448.
[94] T. Tokunaga, S. Matsumoto, H. Ohtani, M. Hasebe, Mater. Trans. (2007) 89–96.